Primosomal protein PriC rescues replication initiation stress by bypassing the DnaA-DnaB interaction step for DnaB helicase loading at *oriC*

Ryusei Yoshida, Kazuma Korogi[1], Qinfei Wu[1], Shogo Ozaki*, and Tsutomu Katayama*

Department of Molecular Biology, Kyushu University Graduate School of Pharmaceutical Sciences, Fukuoka, Japan

[1] These authors equally contributed to this study.
*Corresponding authors

Abstract

In *Escherichia coli*, replisome and replication fork assembly is initiated by DnaB helicase loading at the chromosomal origin *oriC* via its interactions with the DnaA initiator and the DnaC helicase loader. Upon replication fork arrest, the replisome including DnaB dissociates from the stalled fork. Replication fork progression is rescued by primosomal protein PriA- or PriC-dependent pathway in which PriA and PriC promote reloading of DnaB in different mechanisms. However, the mechanism responsible for rescue of blocked replication initiation at *oriC* remains unclear. Here, we found that PriC rescued blocked replication initiation in cells expressing an initiation-specific DnaC mutant, in mutant cells defective in DnaA-DnaB interactions, and in cells containing truncated *oriC* sequence variants. PriC rescued DnaB loading at *oriC* even in the absence of Rep helicase, a stimulator of the PriC-dependent replication fork restart pathway. These and results of *in vitro* reconstituted assays concordantly suggest that this initiation-specific rescue mechanism provides a bypass of the DnaA-DnaB interaction for DnaB loading by PriC-promoted loading of DnaB to the unwound *oriC* region. These findings expand understanding of mechanisms sustaining the robustness of replication initiation and specific roles for PriC in the genome maintenance.

Introduction

Chromosome replication is strictly regulated to ensure successful duplication of the genetic material (Costa & Diffley, 2022; Grimwade & Leonard, 2021; Kasho et al., 2023). In *Escherichia coli*, the ATP-bound form of the replication initiator protein DnaA (ATP-DnaA) forms a higher-order complex with DNA-bending protein IHF at the unique chromosomal origin *oriC*. This complex promotes local unwinding of *oriC* and recruits a pair of DnaB helicases, which are successively loaded to the single-stranded (ss) DNA regions in a bidirectional manner with the aid of DnaC helicase loader. ssDNA-loaded DnaB interacts with DnaG primase and DNA polymerase III holoenzyme, resulting in assembly of the replisome (Arias-Palomo et al., 2019; Chodavarapu & Kaguni, 2016; Hayashi et al., 2020; O'Donnell et al., 2013; Sakiyama et al., 2017, 2018, 2022; Wegrzyn & Konieczny, 2023). Replisomes disassemble when the replication fork stalls in front of an obstacle, such as protein-DNA roadblock or single strand breaks. PriA recognizes the abandoned fork structure, which triggers reloading of DnaB with its partner proteins, such as PriB, PriC, DnaT, and DnaC (Heller & Marians, 2005a; Masai et al., 1994; Michel & Sandler, 2017; Windgassen et al., 2018). In addition, independently of PriA, PriC binds to the abandoned fork structure, triggering reloading of DnaB with the aid of DnaC, which is supported by Rep helicase depending on the fork structure (Heller & Marians, 2005b; Sandler et al., 1999). Also, homologous recombination mechanisms can rescue the abandoned replication fork during SOS responses (Asai & Kogomal, 1994; Kogoma, 1997; Né Dicte Michel et al., 2001). In contrast to these well characterized mechanisms at abandoned forks, little is known about what happens when replication initiation is impeded at *oriC*.

E. coli oriC comprises a Duplex-Unwinding Element (DUE) and a DnaA-Oligomerization Region (DOR) (Figure 1A) (Grimwade & Leonard, 2021; Kasho et al., 2023; Wegrzyn & Konieczny, 2023). The DUE contains 13-mer AT-rich sequence repeats known as L-, M-, and R-DUEs. The M- and R-DUEs are essential for stable DUE unwinding with the specific sequences (TT[A/G]T(T)) used for DnaA-ssDNA binding (Ozaki & Katayama, 2012; Sakiyama et al., 2017). The L-DUE containing the TTATT sequence promotes efficient DnaB loading by expanding the unwound *oriC* region (Sakiyama et al., 2022). The DOR is divided into three subregions: the Left-, Middle-, and Right-DORs, which contain asymmetric 9-mer DnaA binding sequences (DnaA box) with the consensus sequence TTA[T/A]NCACA (Figure 1A) (Noguchi et al., 2015; Ozaki & Katayama, 2012; Rozgaja et al., 2011; Sakiyama et al., 2017; Shimizu et al., 2016). The Left-DOR contains a cluster of unidirectionally aligned DnaA boxes including high-affinity DnaA box R1, and low-affinity boxes R5M, τ1−2, and I1-2, with an IHF-binding region between R1 and R5M boxes. The Right-DOR contains an oppositely oriented DnaA box cluster including high-affinity DnaA box R4 and low-affinity boxes I3 and C1-3. These DnaA box clusters form frameworks for the Left- and Right-DnaA subcomplexes, respectively. DnaA bound to the R2 box, which

solely resides in the Middle-DOR, stabilizes these DnaA subcomplexes (Miller et al., 2009; Rozgaja et al., 2011; Shimizu et al., 2016). In addition, the AT-cluster (TATTAAAAAGAA) region, which connects to the L-DUE, stimulates DnaB loading in the absence of the Right-DnaA subcomplex (Sakiyama et al., 2022).

DnaA comprises four functional domains (Figure 1B). Domain I binds to multiple proteins such as DnaB helicases and the DnaA-assembly stimulator DiaA (Abe et al., 2007; Hayashi et al., 2020; Keyamura et al., 2007, 2009). Domain II is a flexible linker (Abe et al., 2007; Nozaki & Ogawa, 2008). Domain III contains AAA+ (ATPases Associated with various cellular Activities) motifs, which are involved in tight ATP/ADP binding, ATP hydrolysis, and domain III-III interactions (Duderstadt et al., 2011; Erzberger et al., 2006; Felczak & Kaguni, 2004; Kawakami et al., 2005; Ozaki et al., 2012). The arginine finger motif (Arg285) in domain III interacts with ATP bound to domain III of adjacent DnaA protomers, stimulating DnaA complex formation in a cooperative manner (Kawakami et al., 2005; Noguchi et al., 2015). In addition, H/B motifs (Val 211 and Arg245) in this domain bind to ssDNA in a sequence-specific manner (Ozaki et al., 2008; Sakiyama et al., 2017). Domain IV, which comprises the helix-turn-helix motif, recognizes the DnaA box (Fujikawa et al., 2003).

For replication initiation, ATP-DnaA molecules cooperatively oligomerize at *oriC* to form the Left- and Right-DnaA subcomplexes (Figure 1C). Formation of these complexes is stimulated by homotetrameric DiaA protein, which binds up to four DnaA molecules via domain I, including Phe46 (Keyamura et al., 2007, 2009). In concert with DNA superhelicity and thermal energy, the DUE undergoes initial unstable unwinding, which is stabilized through specific interaction between H/B motifs of domain III in the Left-DnaA subcomplex and the upper strand of M- and R-DUEs. This interaction is facilitated by sharp DNA bending by IHF, resulting in stable DUE unwinding (Figure 1C) (Ozaki et al., 2008; Sakiyama et al., 2017). When the single-stranded region is expanded to the L-DUE, the resultant single-stranded L-DUE binds the H/B motifs within the Right-DnaA subcomplex, maximizing the efficiency of the DnaB loading process (Sakiyama et al., 2022).

Subsequently, two DnaB helicases are loaded onto each ssDUE strand through interactions with DnaC and DnaA (Figure 1D). DnaC binding to DnaB changes the closed ring structure of the DnaB hexamer to an open spiral form to allow it to encircle ssDNA (Arias-Palomo et al., 2019; Nagata et al., 2020). Each Left- and Right-DnaA subcomplex binds a DnaB-DnaC complex via high-affinity interaction between DnaA Phe46 and DnaB Leu160 and guides the DnaB-DnaC complexes to unwound ssDUE strands via a low-affinity interaction between DnaA domain III His136 and DnaB (Figure 1B and 1D). Upon interaction with ssDNA, DnaC dissociates from DnaB, which enables migration of DnaB hexamer with helicase action. The pair of DnaB helicases loaded onto the ssDNA strands progress in opposite directions, forming replisomes with DnaG and Pol III holoenzyme (Chodavarapu & Kaguni, 2016;

101 O'Donnell et al., 2013).

102 Replication restart pathways ensure fork progression of the entire chromosome under conditions
103 that trigger replisome disassembly (Heller & Marians, 2005a; Lopper et al., 2007; Michel & Sandler,
104 2017). PriA helicase-dependent pathways predominantly facilitate DnaB reloading onto abandoned forks
105 *in vivo* (Flores et al., 2002). PriA is a 3'-5' DNA helicase and has specific affinity for forked DNA
106 structures comprising one parental dsDNA and two newly synthesized sister dsDNA strands. This permits
107 PriA recognition of the abandoned replication fork and the subsequent unwinding of the nascent lagging
108 strand (Duckworth et al., 2023; Windgassen et al., 2018; Windgassen & Keck, 2016). The resultant
109 unwound ssDNA associates with PriB and DnaT to promote reloading of DnaB helicase with the aid of
110 DnaC (Duckworth et al., 2023; Heller & Marians, 2005a; Lopper et al., 2007). In the absence of PriB,
111 PriC participates in a PriA-dependent pathway (Sandler et al., 1999). In addition, PriA is required for
112 *oriC*/DnaA-independent chromosomal replication called stable DNA replication (SDR) (Masai et al.,
113 1994), which is promoted by UV irradiation (inducible iSDR) and loss of *rnhA* or *recG* (constitutive
114 cSDR) (Kogoma, 1997). In both mechanisms, replication is initiated at triple-stranded structures
115 comprising a dsDNA-ssDNA hybrid (D-loop) or a dsDNA-ssRNA hybrid (R-loop) generated at specific
116 chromosomal loci. These structures mimic the abandoned fork structure, thereby allowing helicase
117 loading to occur similarly to that during PriA-dependent fork restart (Masai et al., 1994).

118 Independently of PriA, PriC can restart replication from abandoned forks through its interaction
119 with the ssDNA region and SSB (Single-Stranded DNA Binding protein) (Figure 1E) (Heller & Marians,
120 2005a; Wessel et al., 2013, 2016). PriC consists of N-terminal and C-terminal domains, which are
121 composed of α helices and are connected by a short linker. The PriC C-terminal domain remodels the
122 SSB-ssDNA complex, which is a prerequisite for the recruitment of DnaB helicase (Heller & Marians,
123 2005a; Wessel et al., 2013, 2016). PriC also interacts with Rep helicase. When the length of the ssDNA
124 gap within the abandoned fork is short, Rep helps expand the ssDNA gap, promoting PriC-mediated
125 remodeling of the SSB-ssDNA complex (Heller & Marians, 2005a, 2005b; Nguyen et al., 2021). Notably,
126 in addition to these functions at the abandoned forks, PriC is suggested to play a role in DnaA-*oriC*-
127 dependent replication initiation under challenging conditions, as evidenced by the synthetic lethality
128 between *priC303*::*kan* and a subgroup of temperature-sensitive *dnaA* mutant alleles (*dnaA46* and
129 *dnaA508*): i.e. *priC303*::*kan* mutants bearing *dnaA46* or *dnaA508*, but not wild-type (WT) *dnaA*, can not
130 grow even at 30°C (Hinds & Sandler, 2004). However, the mechanisms via which PriC rescues blocked
131 replication initiation remain elusive.

132 In this study, we analyzed the PriC-dependent promotion of replication initiation from *oriC* in
133 the context of various replication initiation stresses. We found that PriC stimulated replication initiation
134 in *dnaC2* cells, in which DnaB helicase loading at *oriC* is defective, indicating that it has a role in the

135 rescue of blocked replication initiation. Moreover, PriC stimulated the growth of cells defective in
136 DnaA-DnaB interactions in addition to the growth of cells with *oriC* sequence deletions that inhibit
137 DnaB loading. Consistent with these results, in an *in vitro* reconstituted system, PriC stimulated DnaB
138 loading when the DnaA-DnaB interaction was inhibited at *oriC*. Furthermore, we found that PriC did
139 not stimulate initiation of cSDR, demonstrating that PriC functions specifically in the DnaA-*oriC*
140 system. Taken together, we suggest that PriC rescues blocks in replication initiation by bypassing DnaB
141 loading at *oriC*-DnaA complexes.
142

143 **Results**

144 **PriC stimulates DNA replication initiation in *dnaA46* and *dnaC2* cells**

145 The temperature-sensitive *dnaA46* and *dnaA508* mutants exhibit synthetic lethality with
146 *priC303*::*kan* even at 30°C (Hinds & Sandler, 2004), suggesting that PriC can rescue blocks in DnaA-
147 dependent replication initiation. However, the mechanism underlying PriC-promoted rescue of blocks in
148 replication initiation remains a mystery. Based on previous reports demonstrating PriC binding to short
149 oligo-ssDNA, SSB, and DnaB and its role in DnaB loading at stalled replication forks (Wessel et al., 2013,
150 2016), we considered the possibility that PriC permits bypass of DnaA-dependent stable DUE unwinding
151 and/or DnaB loading at the *oriC* ssDUE. To genetically test these ideas, we analyzed the impact of PriC
152 on the growth of a temperature-sensitive *dnaC2* mutant, which is competent for ongoing replisome
153 progression at 37–42°C, but defective in DnaB loading specifically at the *oriC* ssDUE (Withers &
154 Bernander, 1998).

155 In spotting assays performed using serial dilutions of the cell cultures and LB agar plates, the
156 cell growth of *dnaA46* cells was slightly inhibited at 37°C (Figure 2A). Consistent with the previous
157 report, when crossed with the Δ*priC* allele, the cell growth of *dnaA46* cells but not WT *dnaA* cells was
158 severely inhibited at 37°C (Figure 2A). Unlike the *dnaA46 priC303*::*kan* cells, the *dnaA46* Δ*priC* cells
159 grew at 30°C without prominent inhibition (Figure 2A). This difference may stem from the different
160 strain backgrounds. Notably, the cell growth of *dnaC2* mutant at 35°C was moderately inhibited,
161 whereas it was severely inhibited in *dnaC2* Δ*priC* double mutant (Figure 2A). Also, the cell growth of
162 *dnaC2* cells and *dnaC2* Δ*priC* cells was similar at 30°C. The observed requirement of PriC for cell
163 growth of *dnaC2* cells at 35°C supports the idea that PriC assists in the DnaC-dependent DnaB loading
164 step at *oriC*.

165 Introduction of a *priC*-encoded plasmid (pBR*priC*), but not an empty vector (pBR322),
166 restored the cell growth of *dnaA46* Δ*priC* double mutant at 37°C (Figure 2-figure supplement 1AB) and
167 that of *dnaC2* Δ*priC* double mutant at 35°C. Also, introduction of pBR*priC* to *dnaA46* and *dnaC2*
168 mutants with intact *priC* (*priC*$^{+}$) might only slightly enhance the cell growth at these temperatures
169 (Figure 2- figure supplement 1AB), suggesting that the intrinsic level of PriC is functionally nearly
170 sufficient.

171 To investigate replication initiation from *oriC*, we used flow cytometry of synchronized cells
172 bearing *dnaA46* or *dnaC2* with or without Δ*priC*. In these experiments, cells were incubated at 42°C or
173 37°C for 80–90 min to synchronize the replication cycle at the pre-initiation step, after which
174 incubation was continued at 30°C for 5 min to allow initiation and then 4 h in the presence of
175 rifampicin and cephalexin to inhibit both replication initiation and cell division and allow replication
176 run-out of the whole chromosome. The resultant number of chromosomes per cell, measured by flow

177 cytometry, is known to correspond to the number of *oriC* copies per cell at the time of drug addition, an
178 indicator of initiation activity.
179 A majority of the synchronized *dnaA46* and *dnaC2* cells had only a single *oriC* copy per cell
180 after incubation at 42°C or 37°C regardless of the presence of Δ*priC* (Figure 2B and 2C). In cells with
181 intact *priC* (*priC*$^+$), after release of initiation at 30°C for 5 min, most cells had two *oriC* copies.
182 However, in *dnaA46* Δ*priC* cells, only about half of the cells had two *oriC* copies after the release
183 (Figure 2B), indicating moderate inhibition of initiation. In *dnaC2* Δ*priC* cells, the number of two-*oriC*
184 cells was slightly lower than that of *dnaC2* cells (Figure 2C). These observations are consistent with the
185 cell growth ability (Figure 2A) and with our hypothesis that PriC contributes to the rescue of blocked
186 replication initiation by assisting DnaB loading onto the *oriC* ssDNA.
187 We further performed flow cytometry analysis to assess the role for PriC in replication
188 initiation of the WT *dnaA/dnaC* cells. To estimate the number of *oriC* copies per unit cell mass
189 (ori/mass) as a proxy for initiation activity (Sakiyama et al., 2017, 2022), exponentially growing cells
190 were subjected to run-out replication in the presence of rifampicin and cefalexin (Figure2-figure
191 supplement 2). When cells were grown in LB medium at 25˚C, 30˚C or 42˚C, the ori/mass values for
192 Δ*priC* mutant were comparable to those of *priC*$^+$ cells. Similar results were observed in cells grown in
193 M9 minimal medium at 30˚C. However, when grown in M9 minimal medium at 37˚C, Δ*priC* mutant
194 cells exhibited slightly reduced ori/mass values. Also, it is noteworthy that in all conditions we tested,
195 the fraction of cells with non-2^n *oriC* copies was slightly higher in Δ*priC* cells compared to *priC*$^+$cells.
196 The asynchronous initiations would be caused by partial inhibition of initiation of multiple origins in
197 Δ*priC* cells, as representatively seen for the case of Δ*priC* cells growing in M9 minimal medium at
198 37°C where four-*oriC* cells reduced and three-*oriC* cells increased, compared to *priC*$^+$ cells. A similar
199 case might be shown for Δ*priC* cells growing in LB medium at 25°C in that eight-*oriC* cells reduced
200 and asynchronous initiations (A.I. %) as well as four-*oriC* cells increased. As such, inhibition of
201 replication initiation would occur intrinsically at low frequency in the WT *dnaA*/*dnaC* background. PriC
202 function would be effective to suppress the inhibition, thereby ensuring replication initiation of multiple
203 origins.
204
205 **PriC rescues the cell growth of DnaA mutants defective in DnaB interactions**
206 DnaA contains two regions for interactions with DnaB during DnaB loading at *oriC* ssDNA:
207 one is a high-affinity region in domain I containing Phe46, and the other is a low-affinity region in
208 domain III containing His136. To analyze the mechanism of PriC-promoted DnaB loading at *oriC*, we
209 introduced a series of pING1 vector-based plasmids encoding WT DnaA (pKA234) or the DnaA F46A
210 H136A double mutant (pFH) into *dnaA46* cells with or without *priC*. Growth of *dnaA46* cells

211 containing pING1 was inhibited at 42°C, but the leaky expression of *dnaA* from pKA234 enabled the
212 growth of these cells, as previously reported (Sakiyama et al., 2018) (Figure 3). Introduction of pFH
213 moderately supported the cell growth of *dnaA46* cells at 42°C. By contrast, *dnaA46* Δ*priC* cells
214 carrying pFH exhibited little growth at 42°C (Figure 3).
215 Western blotting analysis supported that the expression levels of WT DnaA and DnaA F46A
216 H136A proteins in *dnaA46* cells bearing pKA234 or pFH were comparable, regardless of the presence
217 or absence of *priC*$^+$ (Figure 3-figure supplement 1). As DnaA46 is unstable and thermolabile (Shimuta
218 et al., 2004), these cells were grown at 30°C, and were incubated at 42°C for 90 min before Western
219 blotting analysis. The DnaA level in *dnaA46* cells bearing the vector pING1 plasmid was minimum.
220 These results suggest that PriC is crucial for the growth of cells defective in specific DnaA-
221 DnaB interactions, possibly because it can bypass the DnaA-DnaB interaction step required for DnaB
222 loading onto *oriC* ssDNA.
223
224 **PriC rescues DNA replication inhibition by DiaA overexpression *in vivo***
225 DiaA, a homotetrameric protein, binds to multiple DnaA molecules and stimulates DnaA
226 multimer assembly at *oriC* (Keyamura et al., 2007). The Phe46 residue in DnaA domain I is part of the
227 DiaA-binding site and DnaB binding site. Oversupply of DiaA inhibits timely initiation of replication in
228 cells growing in tryptone medium at 30°C, probably because of binding competition between DiaA and
229 DnaB for DnaA domain I (Ishida et al., 2004; Keyamura et al., 2009). If PriC can bypass the DnaA-
230 DnaB interaction requirement for DnaB loading onto *oriC*, PriC should suppress inhibition of initiation
231 by DiaA oversupply. To test this possibility, we introduced pBR322 or its derivative encoding *diaA*
232 (pNA135) into cells with or without *priC* (Figure 4). *priC*$^+$ cells carrying pBR322 or pNA135 similarly
233 grew on LB agar plates containing ampicillin between 25°C and 42°C (Figure 4A and Figure 4-figure
234 supplement 1). However, cell growth of Δ*priC* cells carrying pNA135, but not pBR322, was moderately
235 inhibited at 25°C (Figure 4A), supporting our conjecture that PriC can bypass the requirement for the
236 DnaA-DnaB interaction.
237 Rep helicase stimulates PriC-mediated rescue of arrested replication forks containing nascent
238 strands (Heller & Marians, 2005b, 2005a; Sandler, 2000). To test the contribution of Rep helicase to
239 PriC-promoted rescue of blocked replication initiation, we introduced pBR322 or pNA135 into Δ*rep*
240 cells. Unlike Δ*priC* cells, Δ*rep* cells carrying pNA135 grew similarly to Δ*rep* cells carrying pBR322
241 (Figure 4A), suggesting no involvement of Rep in the PriC-promoted rescue of blocked replication
242 initiation. This is consistent with the features of unwound *oriC*, which has a fork structure similar to
243 that of the replication fork but without nascent strands, and the specific role of Rep in rescuing
244 abandoned replication forks with nascent strands in the PriC-dependent pathway. Rep is specifically

245 required for the unwinding of the nascent leading strand of abandoned replication forks, which is
246 needed to expand the ssDNA region required for entry of PriC (Heller & Marians, 2005b, 2005a).
247 We further analyzed replication initiation in Δ*priC* cells carrying pNA135 at 30°C by flow
248 cytometry (Figure 4B). Under these conditions, *priC*$^{+}$ cells bearing pBR322 mainly had eight or four
249 *oriC* copies per cell with eight-*oriC* cells predominating (Figure 4B). The number of *oriC* copies per
250 cell was similar to that in *priC*$^{+}$ cells bearing pNA135, with only slight increase of asynchronous
251 initiation, as shown by the slight increase in the number of cells with non-2^{n} *oriC* copies, which is
252 basically consistent with our previous data (Ishida et al., 2004). However, in Δ*priC* cells bearing
253 pNA135, severe inhibition of initiation occurred, as shown by the substantial decrease in the number of
254 eight-*oriC* cells and the large increase of the number of cells with only one to three *oriC* copies (Figure
255 4B). This result supports the proposed function of PriC at *oriC* mentioned above.
256 To test whether PriC rescues replication initiation inhibited by deletion of the *diaA* gene, we
257 conducted similar flow cytometry analysis of Δ*priC*, Δ*diaA*, and Δ*priC* Δ*diaA* cells (Figure 4C). Δ*diaA*
258 cells showed severe asynchrony of replication initiation, as shown by the increase in the number of five-
259 to-seven-*oriC* cells, which supports the stimulatory role of DiaA in DnaA-*oriC* complex formation
260 (Figure 4C). However, Δ*priC* Δ*diaA* cells did not show more asynchronization of replication initiation
261 than Δ*diaA* cells, as shown by the similar asynchrony index (A.I.). These results suggest that PriC does
262 not support or bypass DnaA-*oriC* complex formation.
263
264 **PriC stimulates replication initiation in cells with *oriC* sequence truncations**
265 Right DnaA-subcomplex plays a stimulatory role in DnaB helicase loading (Sakiyama et al.,
266 2022; Stepankiw et al., 2009). The loading of two DnaB hexamers at *oriC* ssDNA regions requires
267 multiple steps that depend on the distinct functions of two DnaA subcomplexes (Figure 1): the Left-
268 DnaA subcomplex stably unwinds M-R regions of the DUE and the Right-DnaA subcomplex expands
269 the unwound region to the AT-L region, supporting efficient DnaB helicase loading (Sakiyama et al.,
270 2017, 2022; Yoshida et al., 2023). The expanded ssDNA regions in this open *oriC* complex efficiently
271 promote the loading of one DnaB hexamer onto the lower (A-rich) strand M-R region and a second
272 DnaB hexamer onto the upper (T-rich) strand of the DUE (Fang et al., 1999; Sakiyama et al., 2022). In
273 the absence of the Right-DnaA subcomplex, the AT region of the AT-L region assists in DnaB loading
274 (Sakiyama et al., 2022)
275 To determine whether PriC rescues defects in DnaB loading when the *oriC* sequence is altered
276 to prevent Right-DnaA subcomplex formation, we first assessed the cell growth of cells lacking the
277 Middle- and Right-DOR of *oriC* (Left-*oriC*) (Figure 5A). The Left-*oriC* mutant formed colonies at
278 37°C but showed severe growth defects at 25°C and 30°C (Figure 5B). At 37°C, thermal energy might

279 be sufficient to expand DUE unwinding into the AT region and allow DnaB loading in the absence of
280 the Right-DnaA subcomplex (Sakiyama et al., 2022), but not at 25°C or 30°C. By contrast, the cell
281 growth of the Left-*oriC* Δ*priC* double mutant was markedly compromised at 37˚C and moderately
282 reduced at 25°C and 30°C (Figure 5B). These findings support the idea that PriC functions to rescue
283 defective processes in DnaB loading caused by deletions of the *oriC* sequence that prevent DnaA
284 subcomplex formation.

285 Next, similar experiments were performed using a mutant in which the R4 DnaA box within
286 Right-DOR was substituted with a sequence (R4*Tma*) defective in binding of *E. coli* DnaA (Figure 5A
287 and 5C) (Noguchi et al., 2015; Sakiyama et al., 2022). We reasoned that formation of the Right-DnaA
288 subcomplex would be inhibited by the introduction of R4*Tma* and PriC would be required for robust
289 initiation in this context. As the Left-*oriC* strain, the *priC*$^+$ R4*Tma* strain showed normal cell growth.
290 By contrast, cell growth of the R4Tma Δ*priC* double mutant was impaired moderately at 25°C and
291 slightly at 30°C (Figure 5C), indicating that PriC can rescue the blocked replication initiation caused by
292 the absence of the R4 box. The reduced cell growth of R4*Tma* Δ*priC* strain was alleviated at higher
293 temperatures, similar to the phenotype of the Left-*oriC* mutant.

294 Furthermore, we assessed replication initiation in R4*Tma* cells at 30°C using flow cytometry
295 (Figure 5D). R4*Tma* cells grew slightly slower than WT *oriC* cells and showed clear inhibition of
296 initiation; in contrast to the WT *oriC* strain, the R4*Tma* mutant cell population contained more four-
297 *oriC* cells and fewer eight-*oriC* cells, and showed severe asynchronous initiation. Notably, these
298 negative effects of the R4*Tma* mutation were amplified by deletion of *priC*, i.e., the number of one to
299 three-*oriC* cells increased and the ori/mass ratio was further reduced.

300 We next analyzed the role of PriC in cells lacking the AT-L region of *oriC* (subATL *oriC*)
301 (Figure 6A). L-DUE and the flanking AT region assist in DnaB helicase loading by stimulating *oriC*
302 unwinding, which is essential in a strain defective in Right-DnaA subcomplex formation (Sakiyama et
303 al., 2022). SubATL *oriC* cells and WT *oriC* cells grew similarly on LB agar plates between 25°C and
304 37°C, regardless of the presence of Δ*priC* (Figure 6B). However, flow cytometry analysis revealed that
305 deletion of *priC* specifically inhibited initiation in subATL *oriC* cells (Figure 6C); the number of eight-
306 *oriC* cells was lower while the number of four-to-seven *oriC* cells was higher in subATL *oriC* Δ*priC*
307 cells than in *priC*$^+$ subATL *oriC* cells. Taken together, these results are consistent with the idea that PriC
308 restores initiation and DnaB loading at such truncated *oriC* sequences.

309

310 **PriC loads DnaB at *oriC* unwound by the DnaA complex in an *in vitro* reconstituted system**

311 To analyze the mechanism of PriC rescue of blocked initiation at *oriC*, we assessed PriC activity
312 in an *in vitro* reconstituted system for DnaB loading and DnaB-promoted DNA unwinding using the

313 supercoiled circular form (form I) of the *oriC* plasmid pBS*oriC* and purified proteins, namely DnaA, N-
314 terminally histidine-tagged DnaB (His-DnaB), DnaC, IHF, SSB, and gyrase. In this system, DnaA and
315 IHF unwind the DUE and stimulate His-DnaB loading to the ssDUE region with the aid of DnaC. The
316 loaded His-DnaB expands the ssDNA regions in concert with the ssDNA-binding activities of SSB.
317 Concomitantly, the positive supercoiling generated through DNA unwinding by His-DnaB is resolved by
318 DNA gyrase, resulting in the formation of plasmid DNA topoisomers (form I*). Form I* can be separated
319 from form I by agarose gel electrophoresis (Baker et al., 1986; Sakiyama et al., 2022).
320 First, we assessed the effect of PriC on WT DnaA. WT DnaA stimulated form I* formation in
321 the absence of PriC (Figure 7A, lanes 1 and 5) and increasing concentrations of PriC moderately
322 inhibited WT DnaA-mediated form I* formation (Figure 7A, lanes 5 to 8), probably because of
323 competition between DnaA and PriC for binding to DnaB. Next, we focused on the DnaA F46A H136A
324 double mutant. The DnaA F46A and DnaA H136A mutant proteins alone are reported not to support
325 form I* formation (Keyamura et al., 2009; Sakiyama et al., 2018). Consistently, the DnaA F46A H136A
326 double mutant protein was inactive in form I* formation (Figure 7A, lane 9). However, when PriC was
327 added to the assay, DnaA F46A H136A promoted form I* formation to a level comparable to that of WT
328 DnaA in the presence of PriC (Figure 7A, lanes 5-12 and 7B), indicating that PriC rescues defective
329 DnaB loading by DnaA F46A H136A-*oriC* complexes. These findings are consistent with the idea that
330 PriC can bypass the strict reliance on DnaA-DnaB interactions for DnaB loading at *oriC*.
331 To corroborate this idea, we also determined whether PriC rescues blocked initiation resulting
332 from unstable DUE unwinding. *oriC* complexes containing DnaA V211A cannot bind to the ssDUE and
333 consequently fails in stable DUE unwinding (Ozaki et al., 2008). The DnaA V211A mutant was
334 virtually inactive for form I * formation irrespective of the presence or absence of PriC (Figure 7A,
335 lanes 13-16, and 7B), indicating that PriC cannot efficiently rescue a defect of DUE unwinding.
336 We further evaluated the DnaB loading activity of PriC in the presence of DiaA using a similar
337 *in vitro* reconstituted system. Previously, DiaA was shown to stimulate *oriC* DUE unwinding, but to
338 inhibit form I* formation, because DiaA-DnaA binding competitively inhibits DnaB-DnaA binding; DiaA
339 and DnaB share the same binding site in DnaA domain I (Figures 7C lanes 1, 3, 5, and 7 and 7D)
340 (Keyamura et al., 2009). PriC moderately stimulated form I* formation specifically in the presence of
341 both DnaA and DiaA (Figures 7C lanes 7 and 8, and 7D). These results further support the idea that PriC
342 can bypass the specific requirement for the DnaA-DnaB interaction in DnaB loading at *oriC*. DiaA bound
343 to *oriC*-DnaA complexes might be a physical obstacle reducing efficiency of DnaB loading by PriC.
344 In addition, we analyzed the DUE unwinding activities of DnaA mutants using the *in vitro*
345 reconstituted system. As previously reported, DnaA V211A is largely inactive in DUE unwinding, but
346 DnaA F46A H136A unwinds the DUE at a level comparable to that of WT DnaA (Figure 7-figure

347 supplement 2A and 2B). PriC did not stimulate DUE unwinding irrespective of the presence of WT
348 DnaA (Figure 7-figure supplement 2C and 2D). These results demonstrate the functional specificity of
349 PriC in rescuing failed DnaB loading at *oriC* ssDNA and are consistent with the PriC mechanism
350 mentioned above.
351
352 **Role for PriC in cSDR**
353 Finally, to analyze the role of PriC in other types of replication initiation, we examine whether
354 PriC contributes to the initiation of cSDR, which does not require *dnaA* or *oriC* and is activated in cells
355 lacking *rnhA* or *recG*. Although the PriA-PriB-DnaT primosome complex has previously been reported
356 to be involved in the initiation of cSDR (Heller & Marians, 2006), it is unclear whether PriC has any
357 role in this type of initiation.
358 Unlike *dnaA46* cells, *dnaA46 rnhA*::*cat* double mutant cells grew even at 40°C (Figure 8A),
359 indicating that these cells were engaged in cSDR, as previously reported (Hinds & Sandler, 2004). The
360 cell growth of Δ*priC dnaA46 rnhA*::*cat* triple mutant was severely inhibited at 40°C (Figure 8A),
361 suggesting that PriC contributes to the growth of *dnaA46 rnhA*::*cat* mutant cells.
362 To determine whether PriC contributes to the initiation of *dnaA46-oriC* replication or cSDR,
363 we calculated the relative copy numbers of *oriC* (84.6 min) and *ter* (32.4 min: corresponding to *insQ*)
364 using real-time quantitative PCR (qPCR). The *ypaB* (50.5 min) located at the middle position between
365 *oriC* and *ter* was used as a reference. To calculate the copy number of the chromosomal *ter* region, the
366 preferential initiation site of cSDR (Brochu et al., 2018; Maduike et al., 2014), *dnaA46 rnhA*::*cat* cells
367 growing exponentially at 30°C were shifted to 40°C for 90 min and the copy number before and after
368 incubation at 40°C was calculated. Consistent with the cell growth data (Figure 8A), the *ter* copy
369 number ratio of the *dnaA46 rnhA*::*cat* double mutant increased after 40°C incubation, whereas the copy
370 number ratio of the *dnaA46* mutant expressing WT *rnhA* remained the same (Figure 8B). The *ter* copy
371 number ratio of the *dnaA46 rnhA*::*cat* Δ*priC* triple mutant strain was also increased, indicating that
372 cSDR could occur even in the absence of PriC.
373 To monitor initiation of DnaA-*oriC* replication, we determined the *oriC* copy number ratio
374 (Figure 8B). At the permissive temperature, despite having similar growth rates, the *oriC* copy number
375 ratio of the *dnaA46* Δ*priC* double mutant cells was lower than that of the *dnaA46* single mutant,
376 confirming the importance of PriC for replication initiation in *dnaA46* cells, as shown in Figure 2. In the
377 *priC*$^{+}$*dnaA46 rnhA*::*cat* mutant cells, the *oriC* copy number ratio was reduced, which is explained by
378 activation of cSDR and increase of the relative copy number of the reference *ypaB* locus (50.5 min
379 chromosomal map position). Together, these results suggest the idea that PriC stimulates replication
380 fork progression during cSDR.

To consolidate these findings, we performed the chromosome loci copy-number analysis using whole-genome sequencing. The *dnaA46* cells and its derivative cells were grown exponentially at 30°C, followed by incubation at 40°C for 90 min prior to DNA extraction. In growing WT cells, the highest copy numbers are observed near the *oriC*-proximal region and the lowest are near the *ter*-proximal region, resulting in a coverage bias from *oriC* to *ter* (Brochu et al., 2018; Maduike et al., 2014). However, in *dnaA46* cells incubated at 40˚C, the coverage bias was largely diminished due to the run-out replication (Figure 8-figure supplement 1A). Notably, *dnaA46 rnhA*::*cat* cells incubated at 40˚C exhibited discreate coverage peaks at the preferential initiation sites of cSDR near the *ter* (or *insQ*) region with a decreasing coverage bias to *oriC*. Similar profiles were observed in the Δ*priC* mutant background, supporting the idea that cSDR can occur even in the absence of PriC (Figure 8-figure supplement 1A). Moreover, in the *dnaA46 rnhA*::*cat* background, the absence of *priC* appeared to decrease the coverage level at genomic positions near the 1.3 MB and 4 MB map-positions, which are slightly outside of *ter* and *oriC*, respectively (Figure 8-fugure supplement 1B). This observation may reflect the role for *priC* in the replication fork progression.

396 **Discussion**

397 In growing cells, replication initiation can be blocked under challenging conditions. However,
398 the mechanisms that rescue blocked initiations are largely unknown. To elucidate such mechanisms, we
399 investigated PriC-promoted replication initiation under various challenging conditions. We showed that
400 PriC was necessary for the optimal growth of *dnaC2* cells at the semi-restrictive temperature and for
401 replication initiation even at the permissive temperature (Figure 2), suggesting that PriC contributes to
402 replication initiation rescue in *dnaC2* cells by facilitating DnaB helicase loading at *oriC*. Furthermore,
403 we observed that PriC was necessary for the optimal growth of cells in which the DnaA-DnaB
404 interaction was inhibited by DiaA overexpression or DnaA F46A H136A double mutations (Figures 3
405 and 4). In addition, PriC was stimulatory for the cell growth and replication initiation bearing *oriC*
406 mutations that impair efficient DnaB loading (Figures 5 and 6). These results, together with results of
407 form I* formation assays (Figures 7), suggest that PriC bypasses the need for the DnaA-DnaB
408 interaction by binding to unwound *oriC* DNA and recruiting DnaB to facilitate its loading onto ssDNA
409 (Figure 9). This mechanism is similar to that proposed for the rescue of abandoned replication forks by
410 PriC (Figure 1E).

411 Also, PriC contributes to replication initiation rescue in *dnaA46* cells of 37˚C. It is presumable
412 that DnaA46 protein becomes partially denatured at the sub-permissive temperature of 37˚C. This
413 partial denaturation should impair both origin unwinding and helicase loading, though not to the extent
414 that cell viability is lost. The *priC* deletion should further exacerbate helicase loading defects by
415 inhibiting the bypass mechanism (Figure 9), resulting in the lethality of *dnaA46* cells at this
416 temperature.

417 There might remain an alternative possibility that PriC could stabilize the DnaA-DnaB
418 interaction for recusing the impaired DnaB loading process. However, we believe that this possibility is
419 not very likely. Given that interactions between DnaA and DnaB during DnaB loading to *oriC* are
420 highly dynamic and involve regulated multiple steps, the stabilization of the DnaA-DnaB interaction by
421 PriC, even if it occurs, carries a considerable risk of inhibiting the DnaB loading by constructing
422 abortive complexes. In addition, DnaA-DiaA binding is very tight and stable (Keyamura et al.,2007,
423 2009). Even if WT DnaA and WT DnaB are present, PriC can rescue the initiation defects of *oriC*
424 mutants. Based on these facts and the known characteristics of PriC, it is more reasonable to infer that
425 PriC provides a bypass of DnaB loading at *oriC*, similar to the mechanism at the stalled replication fork
426 (Figures 1E and 9).

427 The finding that PriC failed to stimulate form I* formation in the presence of DnaA V211A,
428 which lacks DUE unwinding activity (Figures 7), provides mechanistic insight into PriC-dependent
429 replication initiation at *oriC*. We propose that PriC-dependent replication initiation possibly begins with

430 the recognition of a stably unwound ssDNA region by PriC (Figure 9). Consistent with this perspective,
431 PriC ssDNA-binding activity and ssDNA regions have been reported to be important for PriC-promoted
432 replication fork rescue (Heller & Marians, 2006; McMillan & Keck, 2024). The failure of PriC to
433 stimulate replication initiation in Δ*diaA* cells (Figure 4C) is also potentially explained by the reduced
434 DUE unwinding caused by destabilization of the DnaA-*oriC* complex in Δ*diaA* cells. Based on this, we
435 suggest that the stably unwound ssDNA region in *oriC* serves as a distinctive feature for PriC-
436 promoting DnaB loading at *oriC* for replication initiation rescue, and distinguishes it from PriA-
437 dependent replication restart, which requires the specific structure of the replication fork DNA
438 consisting of sister dsDNA strands (Heller & Marians, 2005a; Windgassen et al., 2018). Unlike PriA,
439 PriC can interact with the simple ssDNA to reload DnaB (Figure 1E).
440 In this study, we found that cells with DnaA F46A H136A double mutations grew well, but
441 only when the cells expressed PriC. As for the DnaA F46A single mutant, our previous studies show that
442 DnaA F46A has a limited residual activity *in vivo* (unlike *in vitro*), and allows slow growth of cells (Abe et
443 al., 2007). The growth of cells expressing the DnaA H136A single mutant was severely inhibited even
444 when the cells expressed PriC (Sakiyama et al., 2018). The His136 residue is located within the weak,
445 secondary DnaB interaction region in DnaA, and is crucial for DnaB loading onto *oriC* ssDNA.
446 Although domain I in DnaA H136A can stably tether DnaB-DnaC complexes to DnaA complexes on
447 *oriC* (Sakiyama et al., 2018), the complexes fail to load DnaB onto *oriC* ssDNA even in the presence of
448 PriC. It is possible that the interaction between PriC and DnaB is inhibited by stable DnaB binding to
449 DnaA domain I. This idea is consistent with the *in vivo* feature of DnaA F46A single mutant.
450 Conversely, the PriC-DnaB interaction may inhibit the interaction between DnaA domain I and DnaB,
451 as suggested by the inhibitory effect of PriC on DnaB loading *in vitro* in the presence of WT DnaA
452 (Figure 7). However, this inhibitory effect of PriC was not observed *in vivo*, suggesting that PriC-DnaB
453 binding could involve still unknown factors and regulatory mechanisms.
454 PriC supported cSDR-dependent growth in *dnaA46 rnhA*::*cat* double mutant cells without
455 stimulating the initiation of cSDR (Figure 8). In this mutant, cSDR predominantly initiates from the *ter*
456 region, resulting in head-on collisions between the replisome and transcription complexes in *rrn*
457 operons (Maduike et al., 2014). This suggests that in cSDR cells PriC specifically rescues abandoned
458 forks including those generated during head-on conflicts between the replisome and transcription
459 complexes.
460 *Bacillus subtilis* (*B. subtilis*), which expresses a PriA homolog but not a PriC homolog,
461 employs a PriA-independent fork rescue pathway (Bruand et al., 2001). In this pathway, *B. subtilis*
462 DnaC (*Bsu*DnaC) helicase is reloaded using the helicase loader DnaI together with *B. subtilis* DnaB
463 (*Bsu*DnaB) and DnaD coloaders. The ssDNA-binding activity of *Bsu*DnaB has a crucial role in this

464 PriA-independent pathway (Bruand et al., 2005). SsDNA-bound *Bsu*DnaB remodels the SSB-ssDNA
465 complex with DnaD and recruits *Bsu*DnaC. These functions of *Bsu*DnaB are similar to the proposed
466 functions of PriC in replication fork rescue in *E. coli*. In addition, *Bsu*DnaC helicase is recruited to *oriC*
467 by concerted actions of *B. subtilis* DnaA and the DnaD-*Bsu*DnaB complex, which has an essential role
468 in chromosome replication initiation (Jameson & Wilkinson, 2017), suggesting a similar role of
469 *Bsu*DnaB to PriC in *E. coli* cells expressing DnaA F46A H136A. These similarities between PriC and
470 *Bsu*DnaB in these two evolutionarily distant bacterial species suggest that the mechanism of PriC-
471 promoted helicase loading is conserved among bacterial species despite the absence of sequence
472 conservation of PriC and *Bsu*DnaB homologs.
473 Based on our results, we propose the abnormal competition between DnaB and DiaA for
474 DnaA domain I could represent a form of intrinsic replication initiation stress in bacteria with conserved
475 DiaA homologs. This type of stress could also occur in ε-proteobacterial species, such as *Helicobacter*
476 *pylori*, because they express HobA, a DiaA-functional homolog (Natrajan et al., 2007; Zawilak-Pawlik
477 et al., 2011). Similarly, YfdR, encoded by *E. coli* prophages, inhibits replication initiation by competing
478 with DnaB for binding to DnaA domain I (Noguchi & Katayama, 2016), suggesting that such
479 extraneously introduced inhibitors could trigger replication initiation stress.
480 Even in human, ORC1, ORC2, and ORC5, the essential components of the eukaryotic
481 replication initiation complex, are not essential in some cancer cell-lines (Shibata & Dutta, 2020; Struhl
482 et al., 2016), suggesting that mechanisms of replication initiation rescue may also operate beyond the
483 bacterial kingdom. Therefore, further investigation of the initiation rescue processes and the factors
484 involved in diverse organisms from bacteria to human will be important for a full understanding of the
485 common principles and diverse mechanisms that ensure robust initiation of chromosomal DNA
486 replication.

487 **Materials and Methods**

488 **Plasmids, proteins, and strains**

489 The plasmids used in this study are listed in Key Resource Table. pKA234, pKW44-1, pNA135,
490 pBS*oriC*, pET22b(+)-priC, and pTKM601 were described previously (Aramaki et al., 2015; Ishida et
491 al., 2004; Kawakami et al., 2005; Keyamura et al., 2009; Kubota et al., 1997; Ozaki et al., 2008). For
492 the construction of pFH, an alanine substitution was introduced into pH136A with specific mutagenic
493 primer sets using the QuikChange site-directed mutagenesis protocol (Stratagene [Agilent], Agilent, La
494 Jolla, CA, United States) as described previously (Keyamura et al., 2007; Sakiyama et al., 2018).

495 WT DnaA and its derivative proteins were overproduced in *E. coli* strain KA450 from pKA234,
496 pKW44-1, or pFH and purified as described previously (Noguchi et al., 2015; Ozaki et al., 2008;
497 Sakiyama et al., 2017).

498 PriC protein was prepared as previously reported with minor modifications (Aramaki et al., 2013).
499 Briefly, PriC protein was overproduced in *E. coli* strain BL21-codonPlus-RIL by inducing its
500 expression from pET22b(+)-priC using 0.2 mM isopropyl-β-D-1-thiogalactopyranoside (IPTG). The
501 resulting cells were suspended in chilled buffer A (50 mM HEPES-NaOH [pH7.0], 10% sucrose, 1 mM
502 EDTA, 2 mM dithiothreitol (DTT), and 1 mM PMSF) and disrupted by sonication. Proteins in the
503 soluble fraction were precipitated with 0.24 g/mL ammonium sulfate, resuspended in a separation buffer
504 (50 mM imidazole [pH 7.0], 20% glycerol, 2 mM DTT, 1 mM EDTA, and 40 mM ammonium sulfate)
505 and loaded onto a 1 mL HiTrap® SP HP column (Cytiva, Uppsala, Sweden). Bound proteins were
506 eluted with a linear gradient from 0 to 1 M sodium chloride.

507 All *E. coli* strains used in this study are listed in Key Resource Table. KYA018, MIT125,
508 MIT162, SA103, NY20 and NY21 were described previously (Kasho & Katayama, 2013; Noguchi et
509 al., 2015; Noguchi & Katayama, 2016). Strains bearing mutant *oriC* (NY20L and NY20ATL) were
510 constructed using the λRed site-directed recombination system as previously described (Noguchi et al.,
511 2015; Sakiyama et al., 2017, 2022). NY20-frt strain and *oriC* mutant strains (NY21-frt, NY20L-frt, and
512 NY20ATL-frt) were constructed by eliminating *kan* from the NY20 strain and strains NY21, NY20L,
513 and NY20ATL. To remove the kanamycin-resistant cassette (*kan*) from *oriC*, FLP recombinase encoded
514 on pCP20 was used. Elimination of *kan* was verified by checking sensitivity to 50 μg/ml kanamycin in
515 LB agar plates. Δ*priC*::*frt-kan* from JW0456-KC and Δ*rep*::*frt-kan* from JW5604-KC were introduced
516 into MG1655 by P1 transduction, resulting in the construction of KRC002 and FF001, respectively. For
517 construction of other Δ*priC*::*frt-kan* strains (KRC004, KRC005, NY20-*priC*, NY21-*priC*, NY20L-*priC*,
518 NY20ATL-*priC*), P1 phage lysates prepared from KRC002 were used for transduction of strains
519 MIT125, KYA018, NY20-frt, SYM21-frt, NY20L-frt, and NY20ATL-frt. Transductants were screened
520 on LB agar plates containing 50 μg/mL kanamycin. Δ*diaA*::*frt-kan* or *rnhA*::*cat* derivatives (KRC006,

521 MIT125c, and KRC004c) were constructed using a similar protocol except that P1 phage lysates from
522 SA103 (Δ*diaA*::*frt-kan*) or MIT162 (*rnhA*::*cat*) were used. KRC003 was generated by removal of *kan*
523 from KRC002.
524
525 **Buffers**
526 Buffer P contained 60 mM HEPES–KOH (pH 7.6), 0.1 mM zinc acetate, 8 mM magnesium
527 acetate, 30% [v/v] glycerol, and 0.32 mg/mL bovine serum albumin (BSA). Buffer N contained 50 mM
528 HEPES–KOH (pH 7.6), 2.5 mM magnesium acetate, 0.3 mM EDTA, 7 mM DTT, 0.007% [v/v] Triton
529 X-100, and 20% [v/v] glycerol. Form I* buffer contained 20 mM Tris-HCl (pH 7.5), 125 mM potassium
530 glutamate, 10 mM magnesium acetate, 8 mM DTT, and 0.5 mg/mL BSA.
531
532 **DUE unwinding assay**
533 DUE unwinding assays were performed essentially as described with minor modifications
534 (Sakiyama et al., 2022; Yoshida et al., 2023). Briefly, DnaA was incubated with ATP in buffer N on ice
535 for 3 min to generate ATP-DnaA. The indicated amount of PriC and ATP-DnaA or its mutant derivatives
536 was incubated for 9 min at 30°C in 10 μL buffer P containing 5 mM ATP, 125 mM potassium glutamate,
537 1.6 nM pBS*oriC*, and 42 nM IHF, followed by further incubation with 1.5 units of P1 nuclease (Wako)
538 for 5 min. The reaction was stopped by the addition of 1% SDS and 25 mM EDTA, and DNA was
539 purified by phenol-chloroform extraction and ethanol precipitation. One-third of each purified DNA
540 was digested with AlwNI (NEB), which yielded 2.6 kb and 1.0 kb fragments after DUE unwinding of
541 pBS*oriC*. The resultant DNA fragments were analyzed by 1% agarose gel electrophoresis with 1xTris-
542 acetate-EDTA buffer for 30 min at 100 V, followed by ethidium bromide staining. Gel images were
543 taken using the GelDoc GO imaging system (Bio-Rad Laboratories, Hercules, CA), and products
544 derived from unwound plasmids were quantified using ImageJ software.
545
546 **Form I* assay**
547 This assay was performed as previously described with minor modifications (Baker et al.,
548 1986; Noguchi et al., 2015; Sakiyama et al., 2022). The indicated amount of ATP-DnaA was incubated
549 for 15 min at 30°C in 12.5 μL of Form I* buffer containing 3 mM ATP, 1.6 nM pBS*oriC*, 42 nM IHF,
550 400 nM His-DnaB, 400 nM DnaC, 76 nM GyrA, 100 nM His-GyrB, and 760 nM SSB. The reaction
551 was stopped by the addition of 0.5% SDS, and DNA was purified by phenol-chloroform extraction.
552 Samples were analyzed by 0.65% agarose gel electrophoresis with 0.5xTris-borate-EDTA buffer for 15
553 h at 23 V, followed by ethidium bromide staining.
554

555 **Flow cytometry analysis**

556 Flow cytometry analysis was performed essentially as described (Kasho et al., 2014). Briefly,
557 cells were grown at 30°C in LB medium until the absorbance of the culture (A_{600}) reached 0.1. Portions
558 of the cultures were diluted a thousand-fold into 5 ml LB medium and incubated at 30°C until the
559 absorbance of the culture (A_{600}) reached 0.1. The remaining portions were further incubated to
560 determine the doubling time (Td) by measuring A_{600} every 20 min. At A_{600} 0.1, aliquots of the cultures
561 were fixed in 70% ethanol to analyze cell mass using the Multisizer 3 Coulter counter (Beckman
562 Coulter, Brea, CA). The remaining cultures were further incubated for 4 h with 0.3 mg/mL rifampicin
563 and 0.01 mg/mL cephalexin to allow run-out replication of chromosomal DNA. The resultant cells were
564 fixed in 70% ethanol. After DNA staining with SYTOX Green (Thermo Fisher Scientific, Waltham,
565 MA), cellular DNA contents were analyzed on a FACS Calibur flow cytometer (BD Bioscience,
566 Franklin Lakes, NJ). The number of the origins/cell (ori/cell) was determined from the histograms of
567 flow cytometry analysis. The number of ori/cell was divided by the mean cell mass determined by cell
568 mass analysis, resulting in ori/mass ratios. The numbers of cells containing non-2^n copy number of *oriC*
569 were divided by the number of cells containing 2^n copy number of *oriC* to calculate the asynchrony
570 index (A.I.). For the analysis of cells bearing plasmids, LB medium was supplemented with 100 μg/mL
571 ampicillin.

572

573 **Replication initiation frequency test using synchronized cultures**

574 MIT125 (*dnaA46 tnaA*::Tn*10*) cells or its Δ*priC* derivative KRC004 were grown at 30°C, a
575 permissive temperature, in LB medium until the absorbance of the culture (A_{600}) reached 0.04, followed
576 by further incubation for 90 min at 42°C, a restrictive temperature. Aliquots of the cultures were fixed
577 in 70% ethanol as "Synchronization" samples. The remaining cultures were further incubated for 5 min
578 to initiate DNA replication, followed by further incubation for 4 h at 42°C with 0.3 mg/mL rifampicin
579 and 0.01 mg/mL cephalexin to allow run-out replication of chromosomal DNA. The resultant cells were
580 fixed in 70% ethanol as "5 min release" samples. After DNA staining with SYTOX Green (Life
581 Technologies), cellular DNA contents were analyzed on a FACS Calibur flow cytometer (BD
582 Bioscience). Ratios of the origins/cell (ori/cell) were determined from the histograms of flow cytometry
583 analysis.

584 For synchronization of *dnaC2* mutant cells (KYA018 and KRC005), cells were grown in LB
585 medium at 30°C until the A_{600} reached 0.04, followed by further incubation for 80 min at 37°C, at the
586 restrictive temperature. The resulting synchronized cultures were released for 5 min at 30°C and
587 incubated in the presence of 0.3 mg/mL rifampicin and 0.01 mg/mL cephalexin at 30°C to allow run-out
588 of chromosomal DNA replication.

589 **qPCR for analysis of cSDR**

590 Cells of MIT125 (*dnaA46 tnaA*::Tn*10*) cells and MIT125c (*dnaA46 tnaA*::Tn*10 rnhA*::*cat*) or
591 its Δ*priC* derivative KRC004 (*dnaA46 tnaA*::Tn*10* Δ*priC*::*frt-kan*) and KRC004c (*dnaA46 tnaA*::Tn*10*
592 *rnhA*::*cat* Δ*priC*::*frt-kan*) were grown at 30°C in LB medium until the absorbance of the culture (A_{600})
593 reached 0.04 and aliquots of the cultures were withdrawn. The remaining samples were further
594 incubated for 90 min at 40°C and aliquots of the cultures were withdrawn. These samples were boiled
595 for 5 min at 95°C and the genome DNA was extracted. The levels of *oriC* (84.6 min), *ter* (32.4 min),
596 and *ypaB* (50.5 min) were quantified by real-time qPCR using TB Green Premix Ex TaqII (Tli RNaseH
597 Plus) (TaKaRa, Shiga, Japan) and the following primers: ORI_1 and KWoriCRev for *oriC*, qoriK fw and
598 qoriK rev for *ter*, STM419 and STM420 for *ypaB*.

599

600 **Chromosome loci copy-number analysis by whole-genome sequencing**

601 The analysis was performed based on a previous paper with modifications (Brochu et al.,
602 2018). Cells of the *dnaA46* mutant derivatives MIT125 (*dnaA46 tnaA*::Tn*10*), MIT125c (*dnaA46*
603 *tnaA*::Tn*10 rnhA*::*cat*), KRC004 (*dnaA46 tnaA*::Tn*10* Δ*priC*::*frt-kan*) and KRC004c (*dnaA46*
604 *tnaA*::Tn*10 rnhA*::*cat* Δ*priC*::*frt-kan*) were grown exponentially at 30°C in LB medium (50 mL). When
605 the absorbance of the culture (A_{600}) reached 0.04, cells were incubated for 90 min at 40°C and collected
606 by centrifugation. Cell pellets were dissolved by incubation at 37°C for 1h in TE buffer (0.6 mL)
607 containing 0.5% SDS and 25 μg/ml proteinase K, and were mixed with 0.2 mL of buffer containing 4%
608 cetyltrimethylammonium bromide, followed by further incubated for 10 minutes at 65°C, phenol-
609 chloroform extraction and isopropanol precipitation. Precipitates were resuspended in Tris (pH7.5)
610 buffer containing 0.1 mg/ml RNaseA, followed by incubation for 1 hour at 37°C and DNA purification
611 by FastGene Gel/PCR Extraction Kit (Nippon Genetics, Tokyo, Japan). The quality control of genomic
612 DNA, library preparation, and whole-genome sequencing were performed by Rhelixa, Inc. using
613 NEBNext Ultra II DNA Library Prep Kit and Illumina NovaSeq X Plus. The number of reads (150 bp x
614 2 pair-ended) was at least 6.7 M (3.3 M pairs) per sample. The sequence data were analyzed using
615 Galaxy (https://usegalaxy.org) and the coverage plot was generated essentially as described (Ivanova et
616 al., 2015). Briefly, paired-end reads were mapped using the MG1655 reference genome (NC_000913)
617 and the BWA-MEM algorithm, followed by calculation of the number of reads per genome coverage.
618 DNA-sequence data are deposited in the NCBI Sequence Read Archive (Accession number:
619 PRJNA1222470).

620

621 **Immunoblot analysis**

622 The assay was performed as described previously with minor modifications (Kawakami et al.,
623 2005; Sakiyama et al., 2017; Yoshida et al., 2023). Briefly, MIT125 (*dnaA46 tnaA*::Tn*10*) and KRC004
624 (*dnaA46 tnaA*::Tn*10* Δ*priC*::*frt-kan*) cells bearing pING1, pKA234, or pFH were grown at 30°C in LB

625 medium including 100 μg/ml ampicillin until the absorbance of the culture (A_{600}) reached 0.05,
626 followed by incubation at 42°C for 90 min. Cells were harvested by centrifugation and dissolved in
627 SDS sample buffer to adjust the calculated A_{600} of 0.5. Proteins were separated using SDS-12%
628 polyacrylamide gel electrophoresis and were transferred to polyvinylidene difluoride membranes
629 (Millipore) using a semi-dry blotting method (Bio-Rad). After blocking at 30°C for 30 min in 3%
630 gelatin-TBS (3% gelatin, 20 mM Tris–HCl, 500 mM NaCl, pH 7.5), the membrane was incubated
631 overnight at 4°C in 1% gelatin-TTBS (20 mM Tris–HCl, 500 mM NaCl, 0.05% Tween-20, pH 7.5)
632 containing anti-DnaA rabbit antiserum (1:3000). After washing, the membrane was incubated at 30°C
633 for 1 h in 1% gelatin-TTBS containing goat anti-rabbit IgG antibody conjugated to alkaline phosphatase
634 (Bio-Rad), followed by development using AP Conjugate substrate Kit (Bio-Rad).
635
636

Acknowledgments

We are grateful to Drs. Yusuke Akama and Yukari Sakiyama for initial exploratory study related to this work.

Fundings

Japan Society for the Promotion of Science (JSPS KAKENHI) [JP17H03656, JP20H03212 and JP23K27131].

References

Abe, Y., Jo, T., Matsuda, Y., Matsunaga, C., Katayama, T., & Ueda, T. (2007). Structure and function of DnaA N-terminal domains: Specific sites and mechanisms in inter-DnaA interaction and in DnaB helicase loading on *oriC*. *Journal of Biological Chemistry*, *282*(24), 17816–17827. https://doi.org/10.1074/jbc.M701841200

Aramaki, T., Abe, Y., Furutani, K., Katayama, T., & Ueda, T. (2015). Basic and aromatic residues in the C-terminal domain of PriC are involved in ssDNA and SSB binding. *Journal of Biochemistry*, *157*(6), 529–537. https://doi.org/10.1093/jb/mvv014

Aramaki, T., Abe, Y., Ohkuri, T., Mishima, T., Yamashita, S., Katayama, T., & Ueda, T. (2013). Domain separation and characterization of PriC, a replication restart primosome factor in *Escherichia coli*. *Genes to Cells*, *18*(9), 723–732. https://doi.org/10.1111/gtc.12069

Arias-Palomo, E., Puri, N., O'Shea Murray, V. L., Yan, Q., & Berger, J. M. (2019). Physical Basis for the Loading of a Bacterial Replicative Helicase onto DNA. *Molecular Cell*, *74*(1), 173-184.e4. https://doi.org/10.1016/j.molcel.2019.01.023

Asai, T., & Kogomal, T. (1994). MINIREVIEW D-Loops and R-Loops: Alternative Mechanisms for the Initiation of Chromosome Replication in *Escherichia coli*. *Journal of Bacteriology*, *176*(7), 1807–1812. https://journals.asm.org/journal/jb

Baker, T. A., Sekimizu, K., Funnell, B. E., & Kornberg, A. (1986). Extensive Unwinding of the Plasmid Template during Staged Enzymatic Initiation of DNA Replication from the Origin of the Escherichia coli Chromosome. *Cell*, *45*(1), 53–64. https://doi.org/10.1016/0092-8674(86)90537-4.

Brochu, J., Vlachos-Breton, É., Sutherland, S., Martel, M., & Drolet, M. (2018). Topoisomerases I and III inhibit R-loop formation to prevent unregulated replication in the chromosomal *Ter* region of *Escherichia coli*. *PLoS Genetics*, *14*(9). https://doi.org/10.1371/journal.pgen.1007668

Bruand, C., Farache, M., McGovern, S., Ehrlich, S. D., & Polard, P. (2001). DnaB, DnaD and DnaI proteins are components of the *Bacillus subtilis* replication restart primosome. *Molecular Microbiology*, *42*(1), 245–256. https://doi.org/10.1046/j.1365-2958.2001.02631.x

Bruand, C., Velten, M., McGovern, S., Marsin, S., Sérèna, C., Dusko Ehrlich, S., & Polard, P. (2005). Functional interplay between the *Bacillus subtilis* DnaD and DnaB proteins essential for initiation and re-initiation of DNA replication. *Molecular Microbiology*, *55*(4), 1138–1150. https://doi.org/10.1111/j.1365-2958.2004.04451.x

Carr, K. M., & Kaguni, J. M. (1996). The A184V missense mutation of the *dnaA5* and *dnaA46* alleles confers a defect in ATP binding and thermolability in initiation of *Escherichia coli* DNA replication. *Molecular Microbiology*, *20*(6), 1307–1318. https://doi.org/10.1111/j.1365-2958.1996.tb02649.x

Chodavarapu, S., & Kaguni, J. M. (2016). Replication Initiation in Bacteria. *Enzymes*, *39*, 1–30. https://doi.org/10.1016/bs.enz.2016.03.001

Costa, A., & Diffley, J. F. X. (2022). The Initiation of Eukaryotic DNA Replication. *Annu. Rev. Biochem*, *91*, 107–131. https://doi.org/10.1146/annurev-biochem-072321

Duckworth, A. T., Ducos, P. L., McMillan, S. D., Satyshur, K. A., Blumenthal, K. H., Deorio, H. R., Larson, J. A., Sandler, S. J., Grant, T., & Keck, J. L. (2023). Replication fork binding triggers structural

changes in the PriA helicase that govern DNA replication restart in *E. coli*. *Nature Communications*, *14*(1), 1–13. https://doi.org/10.1038/s41467-023-38144-x

Duderstadt, K. E., Chuang, K., & Berger, J. M. (2011). DNA stretching by bacterial initiators promotes replication origin opening. *Nature*, *478*(7368), 209–213. https://doi.org/10.1038/nature10455

Erzberger, J. P., Mott, M. L., & Berger, J. M. (2006). Structural basis for ATP-dependent DnaA assembly and replication-origin remodeling. *Nature Structural and Molecular Biology*, *13*(8), 676–683. https://doi.org/10.1038/nsmb1115

Fang, L., Davey, M. J., & O'donnell, M. (1999). Replisome Assembly at *oriC*, the Replication Origin of *E. coli*, Reveals an Explanation for Initiation Sites outside an Origin. *Molecular Cell*, *4*, 541–553. https://doi.org/10.1016/s1097-2765(00)80205-1

Felczak, M. M., & Kaguni, J. M. (2004). The box VII motif of *Escherichia coli* DnaA protein is required for DnaA oligomerization at the *E. coli* replication origin. *Journal of Biological Chemistry*, *279*(49), 51156–51162. https://doi.org/10.1074/jbc.M409695200

Flores, M. J., Ehrlich, S. D., & Michel, B. (2002). Primosome assembly requirement for replication restart in the *Escherichia coli holDG10* replication mutant. *Molecular Microbiology*, *44*(3), 783–792. https://doi.org/10.1046/j.1365-2958.2002.02913.x

Fujikawa, N., Kurumizaka, H., Nureki, O., Terada, T., Shirouzu, M., Katayama, T., & Yokoyama, S. (2003). Structural basis of replication origin recognition by the DnaA protein. *Nucleic Acids Research*, *31*(8), 2077–2086. https://doi.org/10.1093/nar/gkg309

Grimwade, J. E., & Leonard, A. C. (2021). Blocking, Bending, and Binding: Regulation of Initiation of Chromosome Replication During the *Escherichia coli* Cell Cycle by Transcriptional Modulators That Interact With Origin DNA. *Frontiers in Microbiology*, *12*, 732270. https://doi.org/10.3389/fmicb.2021.732270

Hayashi, C., Miyazaki, E., Ozaki, S., Abe, Y., & Katayama, T. (2020). DnaB helicase is recruited to the replication initiation complex via binding of DnaA domain I to the lateral surface of the DnaB N-terminal domain. *Journal of Biological Chemistry*, *295*(32), 1131–1143. https://doi.org/10.1074/jbc.ra120.014235

Heller, R. C., & Marians, K. J. (2005a). The disposition of nascent strands at stalled replication forks dictates the pathway of replisome loading during restart. *Molecular Cell*, *17*(5), 733–743. https://doi.org/10.1016/j.molcel.2005.01.019

Heller, R. C., & Marians, K. J. (2005b). Unwinding of the nascent lagging strand by Rep and PriA enables the direct restart of stalled replication forks. *Journal of Biological Chemistry*, *280*(40), 34143–34151. https://doi.org/10.1074/jbc.M507224200

Heller, R. C., & Marians, K. J. (2006). Replication fork reactivation downstream of a blocked nascent leading strand. *Nature*, *439*(7076), 557–562. https://doi.org/10.1038/nature04329

Hinds, T., & Sandler, S. J. (2004). Allele specific synthetic lethality between *priC* and *dnaAts* alleles at the permissive temperature of 30°C in *E. coli* K-12. *BMC Microbiology*, *4*, 1–9. https://doi.org/10.1186/1471-2180-4-47

Hwang, D. S., & Kaguni, J. M. (1988). Purification and Characterization of the *dnaA46* Gene Product.

Journal of Biological Chemistry 263(22), 10625–10632.

Ivanova, D., Taylor, T., Smith, S.L. et al. (2015) Shaping the landscape of the *Escherichia coli* chromosome: replication-transcription encounters in cells with an ectopic replication origin. *Nucleic Acids Research,* 43:7865–7877. https://doi.org/10.1093/nar/gkv704

Ishida, T., Akimitsu, N., Kashioka, T., Hatano, M., Kubota, T., Ogata, Y., Sekimizu, K., & Katayama, T. (2004). DiaA, a novel DnaA-binding protein, ensures the timely initiation of *Escherichia coli* chromosome replication. *Journal of Biological Chemistry*, *279*(44), 45546–45555. https://doi.org/10.1074/jbc.M402762200

Jameson, K. H., & Wilkinson, A. J. (2017). Control of initiation of DNA replication in *Bacillus subtilis* and *Escherichia coli*. *Genes*, *8*(1), 22. https://doi.org/10.3390/genes8010022

Kasho, K., Fujimitsu, K., Matoba, T., Oshima, T., & Katayama, T. (2014). Timely binding of IHF and Fis to *DARS2* regulates ATP-DnaA production and replication initiation. *Nucleic Acids Research*, *42*(21), 13134–13149. https://doi.org/10.1093/nar/gku1051

Kasho, K., & Katayama, T. (2013). DnaA binding locus *datA* promotes DnaA-ATP hydrolysis to enable cell cycle-coordinated replication initiation. *Proceedings of the National Academy of Sciences of the United States of America*, *110*(3), 936–941. https://doi.org/10.1073/pnas.1212070110

Kasho, K., Ozaki, S., & Katayama, T. (2023). IHF and Fis as *Escherichia coli* Cell Cycle Regulators: Activation of the Replication Origin *oriC* and the Regulatory Cycle of the DnaA Initiator. *International Journal of Molecular Sciences*, *24*(14), 11572. https://doi.org/10.3390/ijms241411572

Kawakami, H., Keyamura, K., & Katayama, T. (2005). Formation of an ATP-DnaA-specific initiation complex requires DnaA arginine 285, a conserved motif in the AAA+ protein family. *Journal of Biological Chemistry*, *280*(29), 27420–27430. https://doi.org/10.1074/jbc.M502764200

Keyamura, K., Abe, Y., Higashi, M., Ueda, T., & Katayama, T. (2009). DiaA dynamics are coupled with changes in initial origin complexes leading to helicase loading. *Journal of Biological Chemistry*, *284*(37), 25038–25050. https://doi.org/10.1074/jbc.M109.002717

Keyamura, K., Fujikawa, N., Ishida, T., Ozaki, S., Su'etsugu, M., Fujimitsu, K., Kagawa, W., Yokoyama, S., Kurumizaka, H., & Katayama, T. (2007). The interaction of DiaA and DnaA regulates the replication cycle in *E. coli* by directly promoting ATP-DnaA-specific initiation complexes. *Genes and Development*, *21*(16), 2083–2099. https://doi.org/10.1101/gad.1561207

Kogoma, T. (1997). Stable DNA Replication: Interplay between DNA Replication, Homologous Recombination, and Transcription. *MICROBIOLOGY AND MOLECULAR BIOLOGY REVIEWS*, *61*(2), 212–238. https://journals.asm.org/journal/mmbr

Kubota, T., Katayama, T., Ito, Y., Mizushima, T., & Sekimizu, K. (1997). Conformational Transition of DnaA Protein by ATP: Structural Analysis of DnaA Protein, the Initiator of *Escherichia coli* Chromosome Replication. *Biochemical and Biophysical Research Communications*, *232*, 130–135. https://doi.org/10.1006/bbrc.1997.6244

Lopper, M., Boonsombat, R., Sandler, S. J., & Keck, J. L. (2007). A Hand-Off Mechanism for Primosome Assembly in Replication Restart. *Molecular Cell*, *26*(6), 781–793. https://doi.org/10.1016/j.molcel.2007.05.012

Maduike, N. Z., Tehranchi, A. K., Wang, J. D., & Kreuzer, K. N. (2014). Replication of the *Escherichia coli* chromosome in RNase HI-deficient cells: Multiple initiation regions and fork dynamics. *Molecular Microbiology*, *91*(1), 39–56. https://doi.org/10.1111/mmi.12440

Masai, H., Asai, T., Kubota, Y., Arai, K. I., & Kogoma, T. (1994). *Escherichia coli* PriA protein is essential for inducible and constitutive stable DNA replication. *EMBO Journal*, *13*(22), 5338–5345. https://doi.org/10.1002/j.1460-2075.1994.tb06868.x

McMillan, S. D., & Keck, J. L. (2024). Biochemical characterization of *Escherichia coli* DnaC variants that alter DnaB helicase loading onto DNA. *Journal of Biological Chemistry*, *300*(5), 107275. https://doi.org/10.1016/j.jbc.2024.107275

Michel, B., & Sandler, S. J. (2017). Replication restart in bacteria. *Journal of Bacteriology*, *199*(13), e00102-17. https://doi.org/10.1128/JB.00102-17

Miller, D. T., Grimwade, J. E., Betteridge, T., Rozgaja, T., Torgue, J.-C., Leonard, A. C., & Helinski, D. R. (2009). Bacterial origin recognition complexes direct assembly of higher-order DnaA oligomeric structures. *Proceedings of the National Academy of Sciences of the United States of America*, *106*(44), 18479–18484. www.pnas.orgcgidoi10.1073pnas.0909472106

Nagata, K., Okada, A., Ohtsuka, J., Ohkuri, T., Akama, Y., Sakiyama, Y., Miyazaki, E., Horita, S., Katayama, T., Ueda, T., & Tanokura, M. (2020). Crystal structure of the complex of the interaction domains of *Escherichia coli* DnaB helicase and DnaC helicase loader: Structural basis implying a distortion-accumulation mechanism for the DnaB ring opening caused by DnaC binding. *Journal of Biochemistry*, *167*(1), 1–14. https://doi.org/10.1093/jb/mvz087

Natrajan, G., Hall, D. R., Thompson, A. C., Gutsche, I., & Terradot, L. (2007). Structural similarity between the DnaA-binding proteins HobA (HP1230) from *Helicobacter pylori* and DiaA from *Escherichia coli*. *Molecular Microbiology*, *65*(4), 995–1005. https://doi.org/10.1111/j.1365-2958.2007.05843.x

Né Dicte Michel, B., Flores, M.-J., Viguera, E., Grompone, G., Seigneur, M., & Bidnenko, V. (2001). Rescue of arrested replication forks by homologous recombination. *Proceedings of the National Academy of Sciences of the United States of America*, *17*(15), 8181–8188. www.pnas.orgcgidoi10.1073pnas.111008798

Nguyen, B., Shinn, M. K., Weiland, E., & Lohman, T. M. (2021). Regulation of *E. coli* Rep helicase activity by PriC. *Journal of Molecular Biology*, *433*(15), 167072. https://doi.org/10.1016/j.jmb.2021.167072

Noguchi, Y., & Katayama, T. (2016). The *Escherichia coli* cryptic prophage protein YfdR binds to DnaA and initiation of chromosomal replication is inhibited by overexpression of the gene cluster *yfdQ-yfdR-yfdS-yfdT*. *Frontiers in Microbiology*, *7*(MAR), 1–21. https://doi.org/10.3389/fmicb.2016.00239

Noguchi, Y., Sakiyama, Y., Kawakami, H., & Katayama, T. (2015). The Arg fingers of key DnaA protomers are oriented inward within the replication origin *oriC* and stimulate DnaA subcomplexes in the initiation complex. *Journal of Biological Chemistry*, *290*(33), 20295–20312. https://doi.org/10.1074/jbc.M115.662601

Nozaki, S., & Ogawa, T. (2008). Determination of the minimum domain II size of *Escherichia coli* DnaA protein essential for cell viability. *Microbiology*, *154*(11), 3379–3384. https://doi.org/10.1099/mic.0.2008/019745-0

O'Donnell, M., Langston, L., & Stillman, B. (2013). Principles and concepts of DNA replication in bacteria, archaea, and eukarya. *Cold Spring Harbor Perspectives in Biology*, *5*(7), a010108. https://doi.org/10.1101/cshperspect.a010108

Ozaki, S., & Katayama, T. (2012). Highly organized DnaA-*oriC* complexes recruit the single-stranded DNA for replication initiation. *Nucleic Acids Research*, *40*(4), 1648–1665. https://doi.org/10.1093/nar/gkr832

Ozaki, S., Kawakami, H., Nakamura, K., Fujikawa, N., Kagawa, W., Park, S. Y., Yokoyama, S., Kurumizaka, H., & Katayama, T. (2008). A common mechanism for the ATP-DnaA-dependent formation of open complexes at the replication origin. *Journal of Biological Chemistry*, *283*(13), 8351–8362. https://doi.org/10.1074/jbc.M708684200

Ozaki, S., Noguchi, Y., Hayashi, Y., Miyazaki, E., & Katayama, T. (2012). Differentiation of the DnaA-*oriC* subcomplex for DNA unwinding in a replication initiation complex. *Journal of Biological Chemistry*, *287*(44), 37458–37471. https://doi.org/10.1074/jbc.M112.372052

Rozgaja, T. A., Grimwade, J. E., Iqbal, M., Czerwonka, C., Vora, M., & Leonard, A. C. (2011). Two oppositely oriented arrays of low-affinity recognition sites in *oriC* guide progressive binding of DnaA during *Escherichia coli* pre-RC assembly. *Molecular Microbiology*, *82*(2), 475–488. https://doi.org/10.1111/j.1365-2958.2011.07827.x

Sakiyama, Y., Kasho, K., Noguchi, Y., Kawakami, H., & Katayama, T. (2017). Regulatory dynamics in the ternary DnaA complex for initiation of chromosomal replication in *Escherichia coli*. *Nucleic Acids Research*, *45*(21), 12354–12373. https://doi.org/10.1093/nar/gkx914

Sakiyama, Y., Nagata, M., Yoshida, R., Kasho, K., Ozaki, S., & Katayama, T. (2022). Concerted actions of DnaA complexes with DNA-unwinding sequences within and flanking replication origin *oriC* promote DnaB helicase loading. *Journal of Biological Chemistry*, *298*(6), 102051. https://doi.org/10.1016/j.jbc.2022.102051

Sakiyama, Y., Nishimura, M., Hayashi, C., Akama, Y., Ozaki, S., & Katayama, T. (2018). The DnaA AAA+ Domain His136 residue directs DnaB replicative helicase to the unwound region of the replication origin, *oriC*. *Frontiers in Microbiology*, *9*(AUG), 1–17. https://doi.org/10.3389/fmicb.2018.02017

Sandler, S. J. (2000). Multiple Genetic Pathways for Restarting DNA Replication Forks in *Escherichia coli* K-12. *Genetics*, *155*, 487–497. https://academic.oup.com/genetics/article/155/2/487/6048048

Sandler, S. J., Marians, K. J., Zavitz, K. H., Coutu, J., Parent, M. A., & Clark, A. J. (1999). *dnaC* mutations suppress defects in DNA replication- and recombination-associated functions in *priB* and *priC* double mutants in *Escherichia coli* K-12. *Molecular Microbiology*, *34*(1), 91–101. https://doi.org/10.1046/j.1365-2958.1999.01576.x

Shibata, E., & Dutta, A. (2020). A human cancer cell line initiates DNA replication normally in the absence of ORC5 and ORC2 proteins. *Journal of Biological Chemistry*, *295*(50), 16949–16959. https://doi.org/10.1074/jbc.RA120.015450

Shimizu, M., Noguchi, Y., Sakiyama, Y., Kawakami, H., Katayama, T., & Takada, S. (2016). Near-atomic structural model for bacterial DNA replication initiation complex and its functional insights. *Proceedings of the National Academy of Sciences of the United States of America*, *113*(50), E8021–

E8030. https://doi.org/10.1073/pnas.1609649113

Shimuta, T. R., Nakano, K., Yamaguchi, Y., Ozaki, S., Fujimitsu, K., Matsunaga, C., Noguchi, K., Emoto, A., & Katayama, T. (2004). Novel heat shock protein HspQ stimulates the degradation of mutant DnaA protein in *Escherichia coli*. *Genes to Cells*, *9*(12), 1151–1166. https://doi.org/10.1111/j.1365-2443.2004.00800.x

Stepankiw, N., Kaidow, A., Boye, E., & Bates, D. (2009). The right half of the *Escherichia coli* replication origin is not essential for viability, but facilitates multi-forked replication. *Molecular Microbiology*, *74*(2), 467–479. https://doi.org/10.1111/j.1365-2958.2009.06877.x

Struhl, K., Shibata, E., Kiran, M., Shibata, Y., Singh, S., Kiran, S., & Dutta, A. (2016). Two subunits of human ORC are dispensable for DNA replication and proliferation. *eLife*, *5*, e19084. https://doi.org/10.7554/eLife.19084.001

Wegrzyn, K., & Konieczny, I. (2023). Toward an understanding of the DNA replication initiation in bacteria. *Frontiers in Microbiology*, *14*, 1328842. https://doi.org/10.3389/fmicb.2023.1328842

Wessel, S. R., Cornilescu, C. C., Cornilescu, G., Metz, A., Leroux, M., Hu, K., Sandler, S. J., Markley, J. L., & Keck, J. L. (2016). Structure and function of the PriC DNA replication restart protein. *Journal of Biological Chemistry*, *291*(35), 18384–18396. https://doi.org/10.1074/jbc.M116.738781

Wessel, S. R., Marceau, A. H., Massoni, S. C., Zhou, R., Ha, T., Sandler, S. J., & Keck, J. L. (2013). PriC-mediated DNA replication restart requires PriC complex formation with the single-stranded DNA-binding protein. *Journal of Biological Chemistry*, *288*(24), 17569–17578. https://doi.org/10.1074/jbc.M113.478156

Windgassen, T. A., & Keck, J. L. (2016). An aromatic-rich loop couples DNA binding and ATP hydrolysis in the PriA DNA helicase. *Nucleic Acids Research*, *44*(20), 9745–9757. https://doi.org/10.1093/nar/gkw690

Windgassen, T. A., Leroux, M., Satyshur, K. A., Sandler, S. J., & Keck, J. L. (2018). Structure-specific DNA replication-fork recognition directs helicase and replication restart activities of the PriA helicase. *Proceedings of the National Academy of Sciences of the United States of America*, *115*(39), E9075–E9084. https://doi.org/10.1073/pnas.1809842115

Withers, H. L., & Bernander, R. (1998). Characterization of *dnaC2* and *dnaC28* Mutants by Flow Cytometry. *JOURNAL OF BACTERIOLOGY*, *180*(7), 1624–1631. https://journals.asm.org/journal/jb

Yoshida, R., Ozaki, S., Kawakami, H., & Katayama, T. (2023). Single-stranded DNA recruitment mechanism in replication origin unwinding by DnaA initiator protein and HU, an evolutionary ubiquitous nucleoid protein. *Nucleic Acids Research*, *51*(12), 6286–6306. https://doi.org/10.1093/nar/gkad389

Zawilak-Pawlik, A., Donczew, R., Szafrański, S., MacKiewicz, P., Terradot, L., & Zakrzewska-Czerwińska, J. (2011). DiaA/HobA and DnaA: A pair of proteins co-evolved to cooperate during bacterial orisome assembly. *Journal of Molecular Biology*, *408*(2), 238–251. https://doi.org/10.1016/j.jmb.2011.02.045

880 **Figure legend**

881 **Figure 1 Schematic structures of *oriC* and DnaA and the replication initiation mechanism.**

882 (A) Overall structure of *oriC* with the AT-rich cluster. *oriC* (245 bp) includes the Duplex-Unwinding
883 Element (DUE, purple bar) and the DnaA-Oligomerization Region (DOR, gray bar). DUE is composed
884 of three AT-rich 13-mer repeats termed L, M, and R. Dark purple boxes indicate the specific sequences
885 involved in DnaA-ssDNA binding (TT[A/G]T(T)). The AT-cluster (purple dots) flanking the DUE
886 outside *oriC* is a supplementary unwinding region. The DOR contains 12 DnaA boxes (filled and open
887 arrowheads representing sites with the full consensus TTA[A/T]NCACA sequence and sites with
888 mismatches, respectively) and an IHF-binding region (IBR, green box). The DOR is subdivided into
889 Left, Middle, and Right subregions. (B) Domains of DnaA. Domains I-IV are shown schematically,
890 with amino acid residue numbers shown in each bracket. H/B motifs (V211 and R245, squares) and
891 Arginine finger (R285, triangle) are indicated. The major functions of each domain are described on the
892 right side of the structure. (C) DUE unwinding by the ssDUE recruitment mechanism. DnaA and IHF
893 are indicated by red and green diagrams, respectively. When ATP-DnaA oligomerizes, DUE is unwound
894 unstably by thermal motion and torsional stress. The M/R region of the DUE-upper strand (purple line)
895 binds to R1-DnaA and R5M-DnaA via IHF-induced DNA bending, resulting in stable DUE unwinding.
896 In addition to M/R-DUE, L-DUE is moderately unwound and interacts with the Right-DnaA
897 subcomplex. (D) Mechanism for DnaB loading. Each Left-DnaA and Right-DnaA subcomplex binds to
898 a DnaB hexamer (blue ovals) complexed with DnaC (yellow circles). (E) PriC-dependent fork rescue
899 pathways. PriC (vivid red circle) promotes DnaB reloading to the abandoned fork, which exposes
900 ssDNA regions. PriC binds to ssDNA at the replication fork, which remodels the SSB-ssDNA complex
901 (for simplicity, SSB is omitted) for DnaC-dependent reloading of DnaB (*upper panel*). If the ssDNA
902 region is accompanied with a nascent lagging strand, Rep helicase (green shape) is recruited by PriC
903 and unwinds the lagging strand to expose the ssDNA region for DnaB loading (the lower case).

904

905 **Figure 2. Requirement of *priC* for DNA replication initiation in *dnaA46* and *dnaC2* strains.**

906 (A) Cell growth abilities. MG1655 and its derivatives MIT125 (MG1655 *dnaA46 tnaA*::Tn*10*), KYA018
907 (MG1655 *dnaC2 zjj18*::*cat*), KRC002 (MG1655 Δ*priC*::*frt-kan*), KRC004 (MG1655 *dnaA46 tnaA*::Tn*10*
908 Δ*priC*::*frt-kan*), and KRC005 (MG1655 *dnaC2 zjj18*::*cat* Δ*priC*::*frt-kan*) were grown overnight. 10-fold-
909 serial dilutions of the overnight cultures (~10^9 cells/mL) were incubated for 16 h at 30°C, or for 14 h at
910 35/37/42°C on LB agar medium. Three independent experiments were performed. +, WT *priC*; -,
911 Δ*priC*::*frt-kan*. The images of representative plates are shown.

912 (B) DNA replication initiation in synchronized *dnaA46* cells with or without *priC*. Exponentially growing
913 MIT125 (MG1655 *dnaA46 tnaA*::Tn*10*) (+) and KRC004 (MG1655 *dnaA46 tnaA*::Tn*10* Δ*priC*::*frt-kan*)

914 (-) cells were synchronized to the pre-initiation stage by incubation for 90 min at 42°C in LB medium,
915 followed by incubation for 5 min at 30°C to initiate DNA replication, which was further followed by
916 incubation with rifampicin and cephalexin for 4 h at 42°C to allow run-out of ongoing DNA replication.
917 Samples were withdrawn after synchronization and run-out replication. The DNA contents of these
918 samples were measured by flow cytometry. Representative histograms of three independent experiments
919 are shown. For each sample, the mean number of cells with more than one chromosome equivalent after
920 a 5 min release was quantified and is shown as a percentage with standard deviations.
921 (C) DNA replication initiation in synchronized *dnaC2* cells with or without *priC*. Exponentially growing
922 KYA018 (MG1655 *dnaC2 zjj18*::*cat*) (+) and KRC005 (MG1655 *dnaC2 zjj18*::*ca* Δ*priC*::*frt-kan*) (-) cells
923 were synchronized to the pre-initiation stage by incubation for 80 min at 37°C in LB medium, followed
924 by incubation for 5 min at 30°C and further incubation with rifampicin and cephalexin as described above.
925 Samples were withdrawn and analyzed as described above.
926
927 **Figure 3. Role of PriC in growth of DnaA mutant defective in interactions with DnaB.**
928 Cell growth of MIT125 (MG1655 *dnaA46 tnaA*::Tn*10*) and KRC004 (MG1655 *dnaA46 tnaA*::Tn*10*
929 Δ*priC*::*frt-kan*) cells bearing pING1 plasmid vector (-) or its derivatives pKA234 expressing WT DnaA
930 (WT) or pFH expressing DnaA F46A H136A (F46A H136A). Cells were grown at 30°C overnight and
931 10-fold-serial dilutions of the cultures (~10^9 cells/mL) were incubated on LB agar plates containing
932 ampicillin for 16 h at 30°C and for 14 h at 42°C, respectively. Four independent experiments were
933 performed. +, WT *priC*; -, Δ*priC*::*frt-kan*.
934
935 **Figure 4. PriC stimulation of DNA replication initiation inhibited by DiaA oversupply.**
936 (A) Cell growth of MG1655, KRC002 (MG1655 Δ*priC*::*frt-kan*), and FF001 (MG1655 Δ*rep*::*frt-kan*)
937 cells bearing pBR322 or pNA135 (pBR322 derivatives carrying *diaA*). Overnight cultures (~10^9
938 cells/mL) of MG1655 and KRC002 cells bearing pBR322 or pNA135 were 10-fold serially diluted and
939 incubated on LB agar plates containing ampicillin for 40 h at 25°C. The results of three independent
940 experiments were consistent, and one which is shown.
941 (B) Flow cytometry analyses of MG1655 and KRC002 (MG1655 Δ*priC*::*frt-kan*) cells bearing pBR322
942 or pNA135. Cells were exponentially grown at 30°C in LB medium with ampicillin, followed by further
943 incubation with rifampicin and cephalexin to allow run-out of chromosomal DNA replication. DNA
944 contents were quantified by flow cytometry, and cell size (mass) at the time of drug addition was
945 measured by a Coulter counter. Mean mass, ori/mass ratio, doubling time (Td), and asynchrony index
946 (A.I.: the percentage of cell numbers with non-2^n copies of *oriC* per the cell numbers with 2^n copies of
947 *oriC*) of each strain are indicated at the top right of each panel with standard deviations. Three to four

948 independent experiments were performed. +, WT *priC*; -, Δ*priC*::*frt-kan*.
949 (C) Flow cytometry analyses of MG1655, KRC003 (MG1655 Δ*priC*::*frt*), SA103 (MG1655 Δ*diaA*::*frt-*
950 *kan*), and KRC006 (MG1655 Δ*priC*::*frt*, Δ*diaA*::*frt-kan*) cells. Cells were grown and analyzed as
951 described above. Three independent experiments were performed. For "*priC*" column, +, WT *priC*; -,
952 Δ*priC*::*frt.* For "*diaA*" column, +, WT *diaA*; -, Δ*diaA*::*frt-kan.*
953
954 **Figure 5. Stimulation of replication initiation by PriC in Right-DnaA subcomplex-defective cells**
955 (A) Schematic structure of Left-*oriC* and R4*Tma oriC.* AT-rich region, DUE, and DOR are indicated by
956 a gray dotted box, a gray box, and an open box, respectively. Filled and open arrowheads in the DOR
957 show DnaA boxes with the full consensus sequence or mismatches. In addition, a striped box indicates
958 the IBR. The regions of each mutant *oriC* are indicated below the structure as open boxes. The position
959 of the *Tma*DnaA box substitution is indicated by a yellow arrowhead.
960 (B) Cell growth of WT *oriC* and Left-*oriC* cells with or without *priC*. Overnight cultures (~10^9 cells/mL)
961 of NY20-frt (WT *oriC*; WT) and NY20L-frt (Left-*oriC*; Left) cells with (+) or without (-) *priC* were 10-
962 fold serially diluted and incubated on LB agar plates for 24 h at 25°C, for 16 h at 30°C, and for 14 h at
963 37°C. +, WT *priC*; -, Δ*priC*::*frt-kan*. Three independent experiments were performed.
964 (C) Cell growth of WT *oriC* and *oriC* R4-box mutant cells with or without *priC*. NY20-frt (WT *oriC*)
965 and NY24-frt (*oriC* with R4*Tma* substitution, R4*Tma*) cells with (+) or without (-) *priC* were grown as
966 described in panel A. +, WT *priC*; -, Δ*priC*::*frt-kan*. Four independent experiments were performed.
967 (D) Flow cytometry analyses of WT and R4*Tma* cells with or without *priC*. Cells were exponentially
968 grown at 30°C in LB medium with ampicillin and analyzed as described in Figure 4. Representative
969 histograms from four independent experiments are shown. Mean mass, ori/mass, and Td of each strain
970 are indicated at the top right of each panel with standard deviations.
971
972 **Figure 6. Stimulation of replication initiation by PriC in cells with a deletion in the ssDNA-**
973 **expanding region of *oriC***
974 (A) Schematic structure of subATL *oriC* as shown in Figure 5. The *oriC* region including the subATL
975 *oriC* is indicated below the structure as a white box.
976 (B) Cell growth of WT *oriC* and *oriC* subATL mutant cells with or without WT *priC*. NY20-frt (WT
977 *oriC*) and NY20ATL-frt (*oriC* lacking AT and L sequences, subATL) with (+) or without (-) WT *priC*
978 were grown as described in Figure 5. +, WT *priC*; -, Δ*priC*::*frt-kan.* Three independent experiments were
979 performed.
980 (C) Flow cytometry analyses of WT *oriC* and *oriC* subATL mutant cells with or without WT *priC*. Cells
981 were exponentially grown at 30°C in LB medium and analyzed as described in Figure 4. Representative

982 histograms from three independent experiments are shown. Mean mass, ori/mass, and Td of each strain
983 are indicated at the top right of each panel with standard deviations.
984
985 **Figure 7. DnaB loading onto the ssDUE by PriC.**
986 (A and B) *In vitro* reconstituted system for DnaB loading. Form I of *oriC* plasmid (pBS*oriC*; 1.6 nM) was
987 incubated for 15 min at 30°C with the indicated amount of PriC in the presence of ATP-DnaA or its mutant
988 derivatives, DnaB, DnaC, IHF, gyrase, and SSB. The resulting plasmids were purified and analyzed using
989 agarose gel electrophoresis. A representative image of three independent experiments is shown in the
990 black/white-inverted mode (A). Band intensities of each lane in the gel image were analyzed by
991 densitometric scanning. The percentages of form I* *oriC* plasmid per input DNA are shown as 'Form I*
992 (%)'. Mean and standard deviations are shown (B). Abbreviations in panel B: -, no addition of DnaA;
993 WT, wild-type DnaA; FH, DnaA F46A H136A; VA, DnaA V211A.
994 (C and D) *In vitro* reconstituted system containing DiaA. Form I of pBS*oriC* plasmid was used as
995 described above except for the addition of the indicated amounts of DiaA. A representative image of three
996 independent experiments is shown in black/white-inverted mode (C). Band intensities of each lane in the
997 gel image were analyzed by densitometric scanning. The percentages of form I**oriC* plasmid together
998 with the mean and standard deviations are shown as described above (D).
999
1000 **Figure 8. PriC stimulation of cSDR-dependent cell growth.**
1001 (A) Cell growth abilities. Cells of MIT125 (MG1655 *dnaA46*), MIT125c (MG1655 *dnaA46 rnhA*::*cat*),
1002 KRC004 (MG1655 *dnaA46* Δ*priC*::*frt-kan*), and KRC004c (MG1655 *dnaA46* Δ*priC*::*frt-kan rnhA*::*cat*)
1003 were grown at 30°C overnight and 10-fold-serial dilutions of the overnight cultures (~10^9 cells/mL) were
1004 incubated for 16 h at 30°C and for 36 h at 40°C on LB agar plates. Three independent experiments were
1005 performed. +, WT; -, deletion.
1006 (B) *oriC* and *ter* copy numbers. MIT125, MIT125c, KRC004, and KRC004c cells growing exponentially
1007 at 30°C were further incubated for 90 min at 40°C in LB medium. Samples were withdrawn before and
1008 after the 40°C incubation. The genome DNA of each sample was extracted by boiling the cells for 5 min
1009 at 95°C. The relative copy numbers of *oriC* (84.6 min) and *ter* (32.4 min) to that of *ypaB* (50.5 min) were
1010 quantified using real-time qPCR. The data and averages of three independent experiments are shown with
1011 standard deviations.
1012
1013 **Figure 9. Model for PriC-promoted replication initiation.**
1014 PriC-promoted rescue of blocked DnaA-*oriC* dependent replication initiation. *oriC*, DnaA, IHF, DnaB,
1015 and DnaC are illustrated as depicted in Figure 1C. When tight DnaA binding of DiaA (dark gray circle)

1016 (or DnaA F46A H136A double mutations) inhibits DnaB recruitment, PriC (Brilliant red circle) binds to
1017 a stably unwound DUE strand, recruiting a DnaB-DnaC complex to lower strand of DUE instead of
1018 Left-DnaA subcomplex. When a sufficient ssDNA region is exposed, PriC then recruits the DnaB-DnaC
1019 complex to the opposite strand.
1020
1021 **Figure 2-figure supplement 1. Role of PriC in cell growth of *dnaA46* and *dnaC2* cells.**
1022 pBR322 vector or pBR322 with *priC* (pBR*priC*) was introduced into cells of MG1655 (*dnaA/dnaC*
1023 WT), KRC002 (MG1655 Δ*priC*::*frt-kan*), MIT125 (MG1655 *dnaA46 tnaA*::Tn*10*), or KRC004
1024 (MG1655 *dnaA46 tnaA*::Tn*10* Δ*priC*::*frt-kan*) (A). The same plasmids were also introduced into cells
1025 of MG1655, KRC002 , KYA018 (MG1655 *dnaC2 zjj18*::*cat*) or KRC005 (MG1655 *dnaC2 zjj18*::*cat*
1026 Δ*priC*::*frt-kan*) (B). Independent transformants were assessed for the cell growth by spotting assays
1027 with incubation at the indicated temperatures for 24 hrs on LB agar plates supplemented with 100 μg/ml
1028 ampicillin as described for Figure 2A.
1029
1030 **Figure 2-figure supplement 2. Role of PriC in cell growth of cells with WT DnaA and DnaC.**
1031 (A) Flow cytometry analyses of MG1655 and KRC002 (MG1655 Δ*priC*::*frt-kan*) cells in LB medium.
1032 Cells were exponentially grown at 25°C, 30°C, and 42°C in LB medium, followed by further incubation
1033 with rifampicin and cephalexin to allow run-out replication of chromosomal DNA. DNA contents were
1034 quantified by flow cytometry, and cell size (mass) at the time of drug addition was measured by a Coulter
1035 counter. Mean mass, ori/mass ratio, doubling time (Td), and asynchrony index (A.I.: the percentage of
1036 cell numbers with non-2^n copies of *oriC* per the cell numbers with 2^n copies of *oriC*) of each strain are
1037 indicated at the top right of each panel with standard deviations. Three to four independent experiments
1038 were performed. +, WT *priC*; -, Δ*priC*::*frt-kan*.
1039 (B) Flow cytometry analyses of MG1655 and KRC002 (MG1655 Δ*priC*::*frt-kan*) cells in M9 minimal
1040 medium including 0.2% glucose and 0.2% casamino acids. Cells were grown and analyzed as described
1041 above. Three independent experiments were performed. For "*priC*" column, +, WT *priC*; -, Δ*priC*::*frt.*
1042
1043 **Figure 3-figure supplement 1. Immunoblot analysis for plasmid encoded DnaA proteins in *dnaA46***
1044 **cells.**
1045 (A and B) Cells of MIT125 (MG1655 *dnaA46 tnaA*::Tn*10*) and KRC004 (MG1655 *dnaA46 tnaA*::Tn*10*
1046 Δ*priC*::*frt-kan*) bearing pING1 (Vector), pKA234 (WT) or pFH (FH) were grown in LB mediium
1047 including ampicillin at 30°C until the absorbance of the culture (A_{600}) reached 0.05, followed by
1048 incubation at 42°C for 90 minutes. Immunoblot analysis was performed using anti-DnaA serum. Purified
1049 DnaA was also used as a quantitative standard. MW, molecular weight markers. A representative

1050 membrane image from three independent experiments is shown (A). Band intensities of each lane in the
1051 image were analyzed by densitometric scanning and the amounts of DnaA were deduced using the
1052 standard and shown as 'DnaA (ng)' (B). Means and standard deviations (SDs) are shown with each data.
1053
1054 **Figure 4-figure supplement 1. Cell growth ability of cells carrying pBR322 or pNA135 with WT**
1055 ***priC* or Δ*priC*::*frt-kan*.**
1056 Cell growth of MG1655 or KRC002 (MG1655 Δ*priC*::*frt-kan*) cells bearing pBR322 or pNA135
1057 (pBR322 derivatives carrying *diaA*). Overnight cultures (~10^9 cells/mL) of MG1655 and KRC002 cells
1058 carrying pBR322 or pNA135 were 10-fold serially diluted and incubated on LB agar plates containing
1059 ampicillin for 14 h at 30–42°C. +, WT *priC*; -, Δ*priC*::*frt-kan*. The results of three independent
1060 experiments were consistent, and one representative result is shown.
1061
1062 **Figure 7-figure supplement 1. DUE unwinding activities of DnaA mutant derivatives in the presence**
1063 **and absence of PriC.**
1064 (A and B) *in vitro* DUE unwinding assays using DnaA mutant derivatives. Form I of *oriC* (pBS*oriC*; 1.6
1065 nM) was incubated for 9 min at 30°C with the indicated amount of DnaA or its mutant derivatives in the
1066 presence of IHF (42 nM), followed by incubation with P1 nuclease (1.5 units) and further incubation with
1067 AlwNI before agarose gel electrophoresis. Note that 2.6 kb and 1.0 kb fragments are observed with
1068 restriction enzyme digestion when the ssDNA-specific P1 nuclease cleaves 3.6 kb pBS*oriC* at the DUE.
1069 A representative image of two independent experiments is shown in black/white-inverted mode (A). The
1070 sizes of each band are indicated at the left side of the image. Bands intensities of each lane in the gel
1071 image were analyzed by densitometric scanning. The percentages of P1 nuclease-digested *oriC* DNA per
1072 input DNA molecules are shown as 'DUE unwinding (%)'. Mean and data are shown (B). Abbreviations
1073 in panel B: -, no addition of DnaA; WT, wild-type DnaA; FH, DnaA F46A H136A; VA, DnaA V211A.
1074 (C and D) *In vitro* DUE unwinding assay with PriC. pBS*oriC* was used as described above except for
1075 PriC addition. A representative image of two independent experiments is shown in black/white-inverted
1076 mode (C). Data were analyzed as described above (D). n.t., not tested.
1077
1078 **Figure 8-figure supplement 1. Chromosome loci copy-number analysis of *dnaA46* mutant cells and**
1079 **its derivative cells.**
1080 (A) Coverage of aligned sequence reads. MIT125, MIT125c, KRC004, and KRC004c cells were
1081 exponentially grown in LB medium at 30°C, followed by incubation for 90 min at 40°C. Chromosomal
1082 DNA from each sample was extracted and analyzed using whole-genome sequencing. Coverage was
1083 calculated for every 250-bp window and plotted, with the coverage at the *oriC* region normalized to 1.0.

1084 Dotted splines represent coverage profiles based on the combined data from two biological replicates,
1085 shown in different colors (red and blue).
1086 (B) Relative coverage. The coverage for each 250-bp window in *priC*$^{+}$ cells was divided by that in
1087 Δ*priC* cells, and the resulting values were plotted as "relative coverage." Yellow lines indicate a value
1088 of 1.0.
1089

Key Resources Table				
Reagent type (species) or resource	**Designation**	**Source or reference**	**Identifiers**	**Additional information**
strain, strain background (*Escherichia coli*)	BW25113 Δ*priC*::*frt-kan*	Keio collection	JW0456-KC	
strain, strain background (*Escherichia coli*)	BW25113 Δ*rep*::*frt-kan*	Keio collection	JW5604-KC	
strain, strain background (*Escherichia coli*)	MG1655 *dnaC2 zjj18*::*cat*	Kasho and Katayama, 2013	KYA018	
strain, strain background (*Escherichia coli*)	MG1655 *dnaA46 tnaA*::Tn10	Noguchi, *et al.*, 2016	MIT125	
strain, strain background (*Escherichia coli*)	MG1655 *rnhA*::*cat*	Noguchi, *et al.*, 2016	MIT162	
strain, strain background (*Escherichia coli*)	MG1655 Δ*diaA*::*frt-kan*	Noguchi, *et al.*, 2016	SA103	
strain, strain background (*Escherichia coli*)	MG1655 Δ*priC*::*frt-kan*	This work	KRC002	MG1655 x P1 JW0456-KC
strain, strain background (*Escherichia coli*)	MG1655 Δ*priC*::*frt*	This work	KRC003	KRC002 x pCP20

strain, strain background (*Escherichia coli*)	MIT125 Δ*priC*::*frt-kan*	This work	KRC004	MIT125 x P1 JW0456-KC
strain, strain background (*Escherichia coli*)	KYA018 Δ*priC*::*frt-kan*	This work	KRC005	KYA018 x P1 JW0456-KC
strain, strain background (*Escherichia coli*)	KRC003 Δ*diaA*::*frt-kan*	This work	KRC006	KRC003 x P1 SA103
strain, strain background (*Escherichia coli*)	MG1655 Δ*rep*::*frt-kan*	This work	FF001	MG1655 x P1 JW5604-KC
strain, strain background (*Escherichia coli*)	MG1655 *asnA*::*frt-kan*	Noguchi, *et al*, 2015	NY20	
strain, strain background (*Escherichia coli*)	MG1655 *asnA*::*frt-kan* *oriC*ΔR4 box::*Tma*DnaA box	Noguchi, *et al*, 2015	NY21	
strain, strain background (*Escherichia coli*)	MG1655 *asnA*::*frt-kan* *oriC*ΔMiddle-Right DOR	This work	NY20L	
strain, strain background (*Escherichia coli*)	MG1655 *asnA*::*frt-kan* *oriC*ΔAT-L region	This work	NY20ATL	

strain, strain background (*Escherichia coli*)	MG1655 *asnA*::*frt*	Yoshida, *et al*, 2023	NY20-frt	
strain, strain background (*Escherichia coli*)	MG1655 *asnA*::*frt* *oriC*ΔR4 box::*Tma*DnaA box	This work	NY21-frt	NY21 x pCP20
strain, strain background (*Escherichia coli*)	MG1655 *asnA*::*frt* *oriC*ΔMiddle-Right DOR	This work	NY20L-frt	NY20L x pCP20
strain, strain background (*Escherichia coli*)	MG1655 *asnA*::*frt* *oriC*ΔAT-L region	This work	NY20ATL -frt	NY20ATL x pCP20
strain, strain background (*Escherichia coli*)	NY20-*frt* Δ*priC*::*frt-kan*	This work	NY20-*priC*	NY20-frt x P1 KRC002
strain, strain background (*Escherichia coli*)	NY21-*frt* Δ*priC*::*frt-kan*	This work	NY21-*priC*	NY21-frt x P1 KRC002
strain, strain background (*Escherichia coli*)	NY20L-*frt* Δ*priC*::*frt-kan*	This work	NY20L-*priC*	NY20L-frt x P1 KRC002
strain, strain background (*Escherichia coli*)	NY20ATL-*frt* Δ*priC*::*frt-kan*	This work	NY20ATL -*priC*	NY20ATL-frt x P1 KRC002

strain, strain background (*Escherichia coli*)	MIT125 Δ*rnhA*::*cat*	This work	MIT125c	MIT125 x P1 MIT162
strain, strain background (*Escherichia coli*)	KRC004 Δ*rnhA*::*cat*	This work	KRC004c	KRC004 x P1 MIT162
antibody	anti-DnaA (Rabbit polyclonal)	Kawakami, *et al.*, 2005		Immunoblot (1:3000)
antibody	Goat Anti-Rabbit IgG (H+L)-AP Conjugate	Bio-Rad	Cat. #1706518	Immunoblot (1:3000)
recombinant DNA reagent	pBR*priC* (Plasmid)	This work		pBR322 encoding *priC*
recombinant DNA reagent	pING1 (Plasmid)	Katayaam, *et al.*, 1994		Vector bearing arabinose-inducible promoter
recombinant DNA reagent	pKA234 (Plasmid)	Kubota, *et al.,* 1997		pING1 encoding *dnaA*
recombinant DNA reagent	pH136A (Plasmid)	Sakiyama, *et al.*, 2018		pKA234 *dnaA* H136A
recombinant DNA reagent	pFH (Plasmid)	This study		pH136A mutated by Quick Change site-directed mutagenesis by primers F46A 1/2
recombinant DNA reagent	pKW44-1 (Plasmid)	Ozaki, *et al.,* 2008		pKA234 *dnaA* V211A

recombinant DNA reagent	pNA135 (Plasmid)	Ishida, *et al.*, 2004		pBR322 bearing *diaA* gene
recombinant DNA reagent	pBS*oriC* (Plasmid)	Kawakami, *et al.* 2005		pBluescript bearing a 678 bp chromosome-derived region including *oriC*
recombinant DNA reagent	pET22b(+)-priC (Plasmid)	Aramaki, *et al.*, 2015		pET22b(+) bearing *priC* under the T7 promoter
recombinant DNA reagent	pTKM601 (Plasmid)	Keyamura, *et al.*, 2007		pBAD/HisB bearing *diaA*
sequence-based reagent	F46A 1	Keyamura *et al.*, 2009	PCR primer	GTACGCGCCAAACCGCGCGGTCCTTCGATTGGGTACG
sequence-based reagent	F46A 2	Keyamura *et al.*, 2009	PCR primer	CGTACCCAATCGAAGGACCGCGCGGTTTGGCGCGTAC
sequence-based reagent	ORI_1	Kasho *et al.*, 2014	qPCR primer	CTGTGAATGATCGGTGATC
sequence-based reagent	KW*oriC*Rev	Kasho *et al.*, 2014	qPCR primer	GTGGATAACTCTGTCAGGAAGCTTG
Sequence-based reagent	qoriK fw	Brochu *et al.*, 2014	qPCR primer	CGAGACTTCAGCGACAGTTAAG
sequence-based reagent	qoriK rev	Brochu *et al.*, 2014	qPCR primer	CCTGCGGATATTTGCGATACA
sequence-based reagent	STM419	This work	qPCR primer	CGGACACCTTGTCTGACCTAAG

sequence-based reagent	STM420	This work	qPCR primer	AGTGTGAAAATGACCC TCTTGC
commercial assay or kit	AP Conjugate Substrate Kit	Bio-Rad	Cat #1706432	

Figure 1

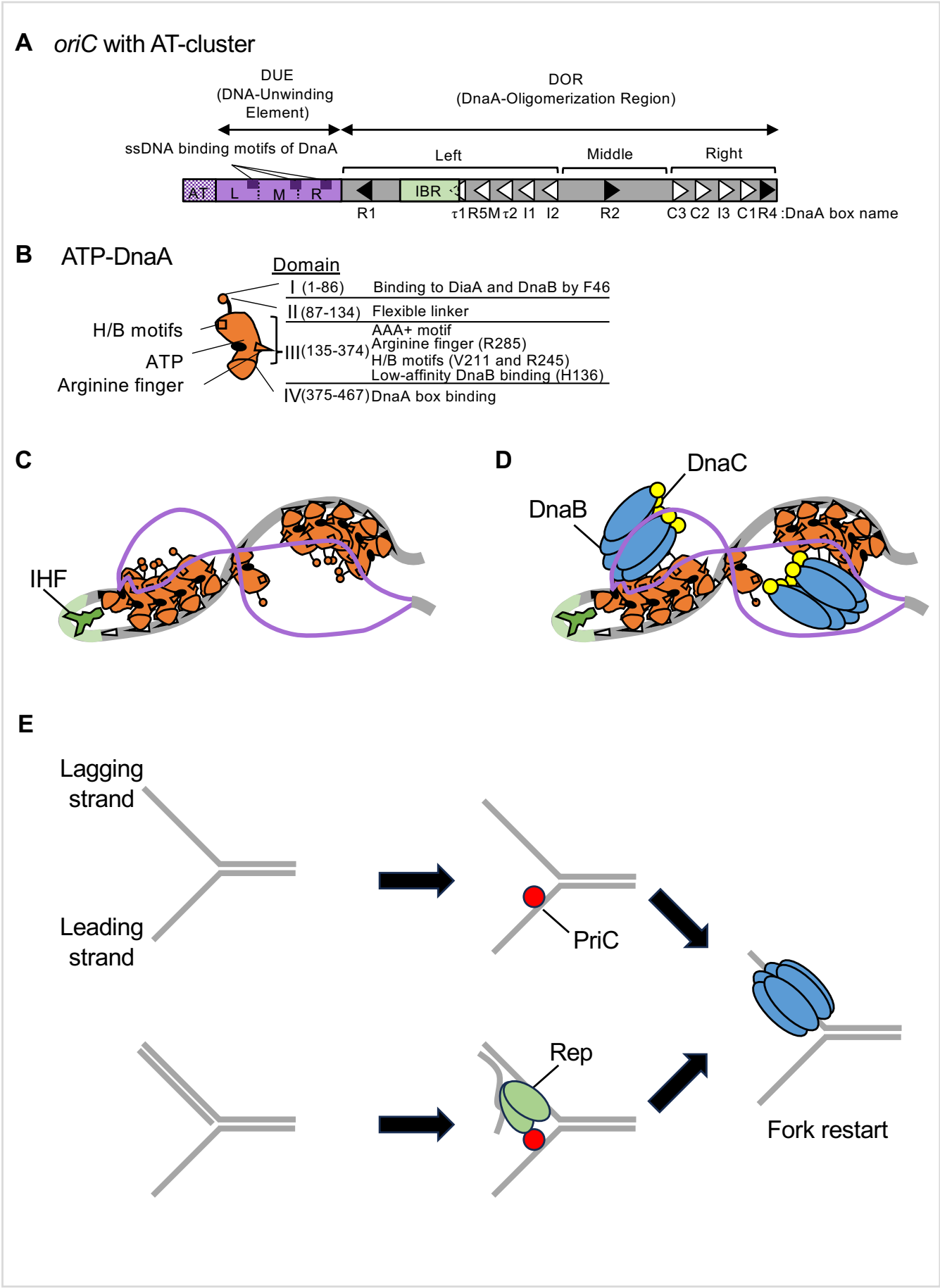
A
oriC with AT-cluster
DUE
(DNA-Unwinding
Element)
DOR
(DnaA-Oligomerization Region)
ssDNA binding motifs of DnaA
Left
Middle
Right
AT
L
M
R
IBR
R1
τ1 R5M τ2 I1 I2
R2
C3 C2 I3 C1R4 :DnaA box name
B
ATP-DnaA
Domain
I (1-86) Binding to DiaA and DnaB by F46
II (87-134) Flexible linker
III(135-374) AAA+ motif
Arginine finger (R285)
H/B motifs (V211 and R245)
Low-affinity DnaB binding (H136)
IV(375-467) DnaA box binding
H/B motifs
ATP
Arginine finger
C
IHF
D
DnaC
DnaB
E
Lagging
strand
Leading
strand
PriC
Rep
Fork restart

Figure 2

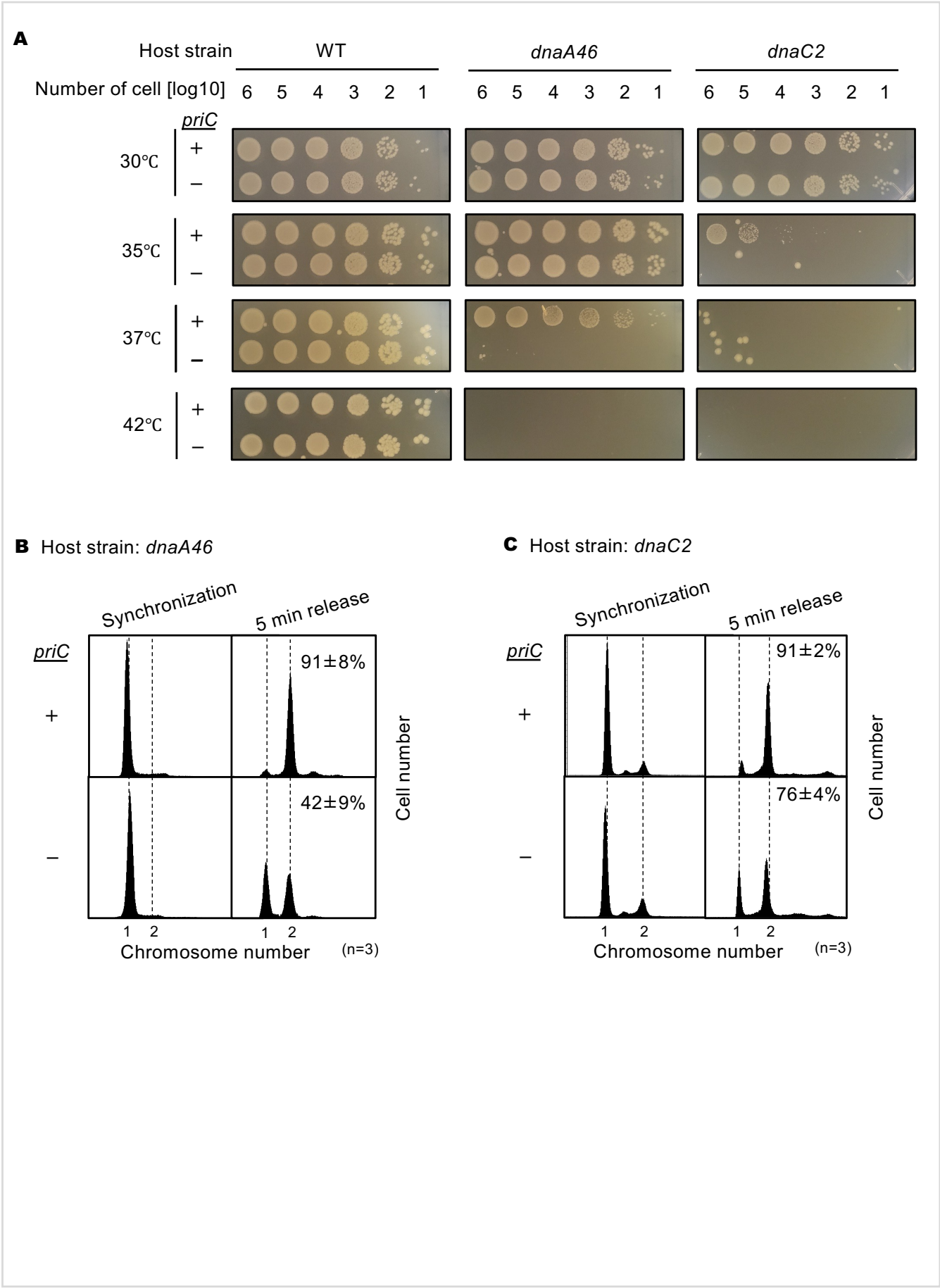
A
Host strain
WT
dnaA46
dnaC2
Number of cell [log10]
6 5 4 3 2 1
priC
30℃
35℃
37℃
42℃
+
−
B Host strain: dnaA46
Synchronization
5 min release
91±8%
42±9%
Cell number
1 2
Chromosome number
(n=3)
C Host strain: dnaC2
91±2%
76±4%

Figure 3

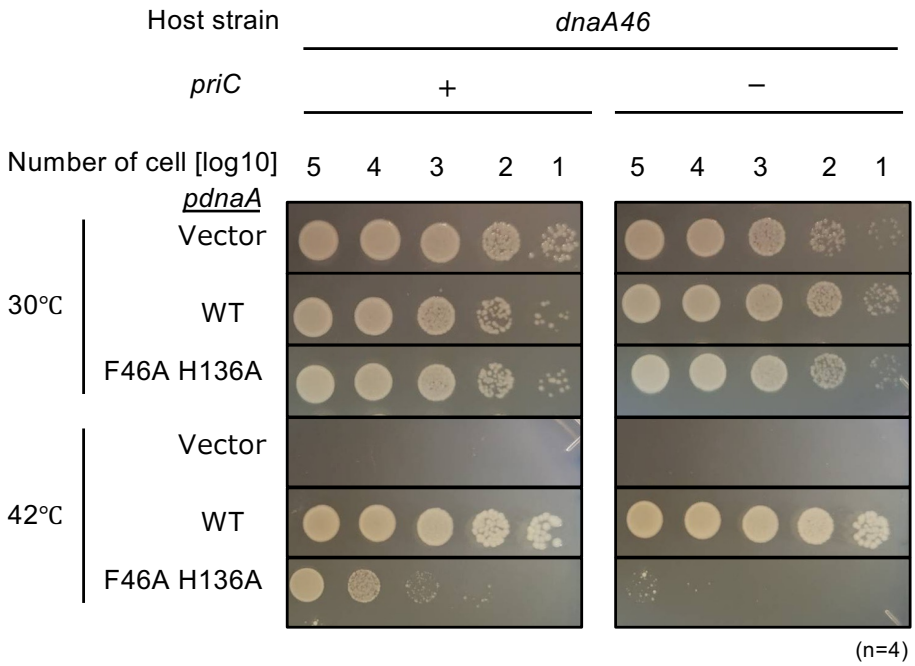
Host strain
dnaA46
priC
+
−
Number of cell [log10]
5 4 3 2 1
5 4 3 2 1
pdnaA
30℃
Vector
WT
F46A H136A
42℃
Vector
WT
F46A H136A
(n=4)

Figure 4

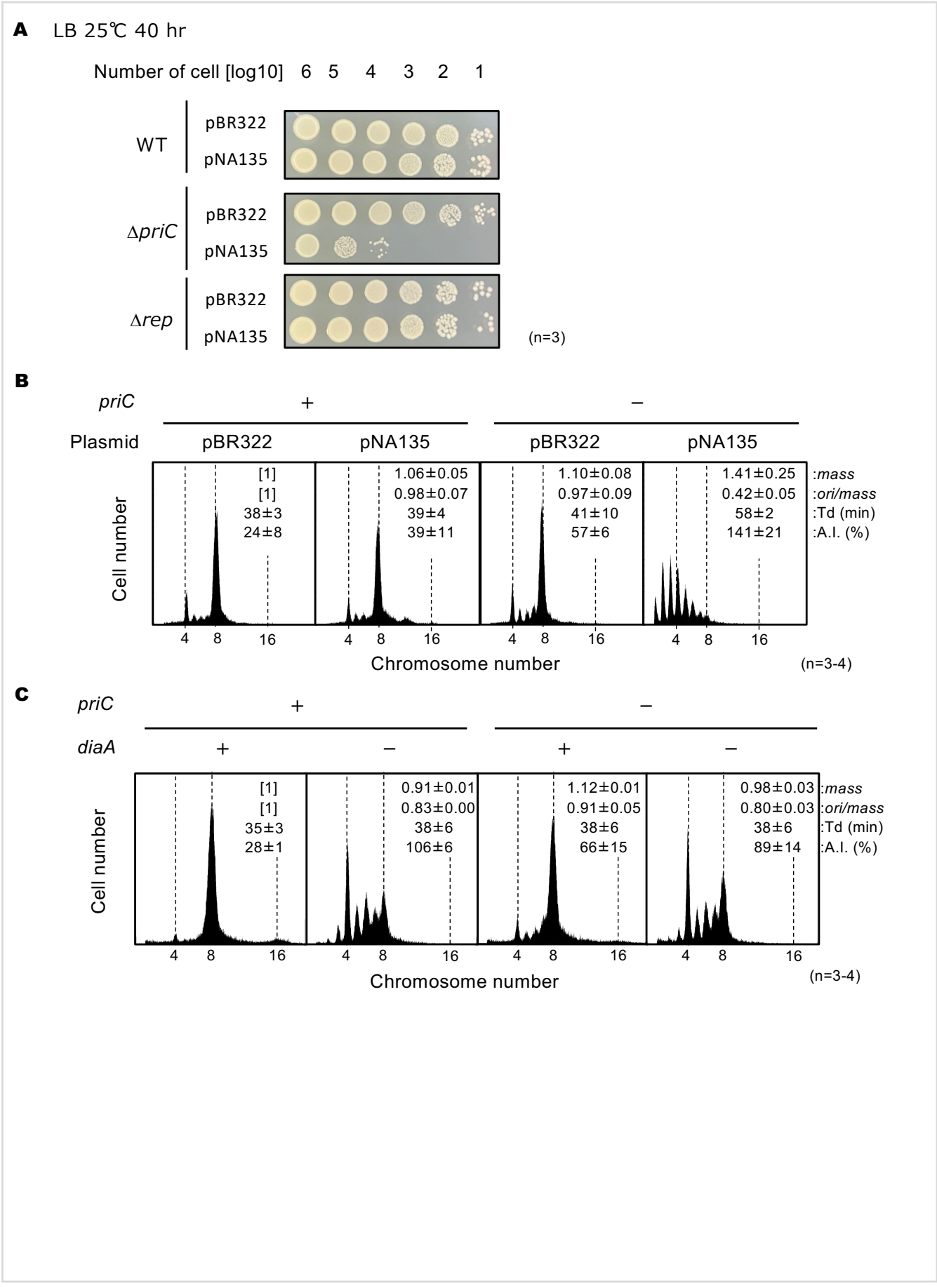
A
LB 25℃ 40 hr
Number of cell [log10] 6 5 4 3 2 1
WT
pBR322
pNA135
ΔpriC
pBR322
pNA135
Δrep
pBR322
pNA135
(n=3)
B
priC
+
−
Plasmid
pBR322
pNA135
pBR322
pNA135
[1]
[1]
38±3
24±8
1.06±0.05
0.98±0.07
39±4
39±11
1.10±0.08
0.97±0.09
41±10
57±6
1.41±0.25
0.42±0.05
58±2
141±21
:mass
:ori/mass
:Td (min)
:A.I. (%)
Cell number
4 8 16
Chromosome number
(n=3-4)
C
priC
+
−
diaA
+
−
+
−
[1]
[1]
35±3
28±1
0.91±0.01
0.83±0.00
38±6
106±6
1.12±0.01
0.91±0.05
38±6
66±15
0.98±0.03
0.80±0.03
38±6
89±14
:mass
:ori/mass
:Td (min)
:A.I. (%)
Cell number
4 8 16
Chromosome number
(n=3-4)

Figure 5

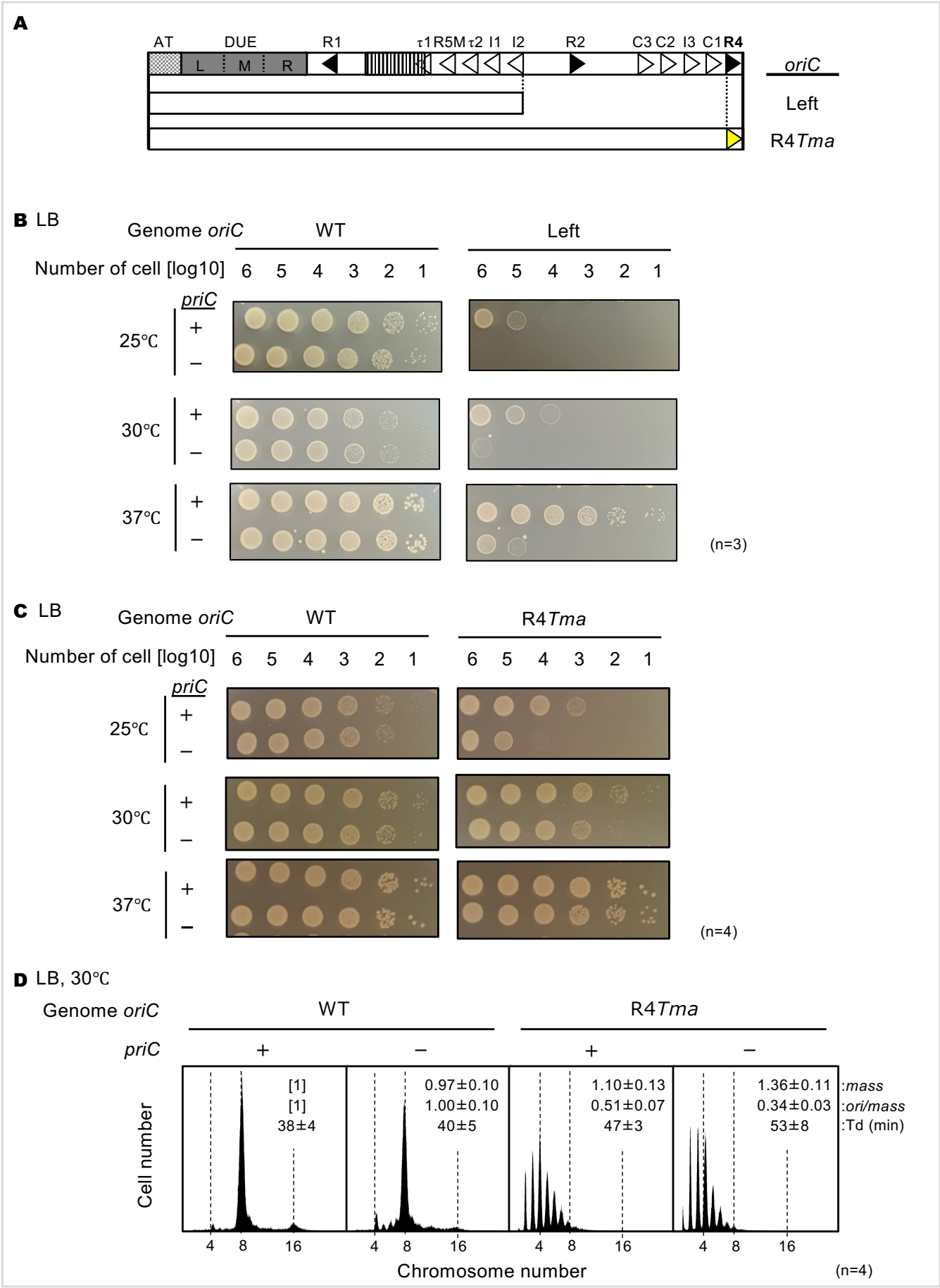
A
AT
DUE
R1
τ1 R5M τ2 I1 I2
R2
C3 C2 I3 C1 R4
L
M
R
oriC
Left
R4Tma
B LB
Genome oriC
WT
Left
Number of cell [log10]
6 5 4 3 2 1
priC
25℃
30℃
37℃
+
−
(n=3)
C LB
Genome oriC
WT
R4Tma
Number of cell [log10]
6 5 4 3 2 1
priC
25℃
30℃
37℃
+
−
(n=4)
D LB, 30℃
Genome oriC
WT
R4Tma
priC
+
−
+
−
[1]
[1]
38±4
0.97±0.10
1.00±0.10
40±5
1.10±0.13
0.51±0.07
47±3
1.36±0.11
0.34±0.03
53±8
:mass
:ori/mass
:Td (min)
Cell number
4 8 16
Chromosome number
(n=4)

Figure 6

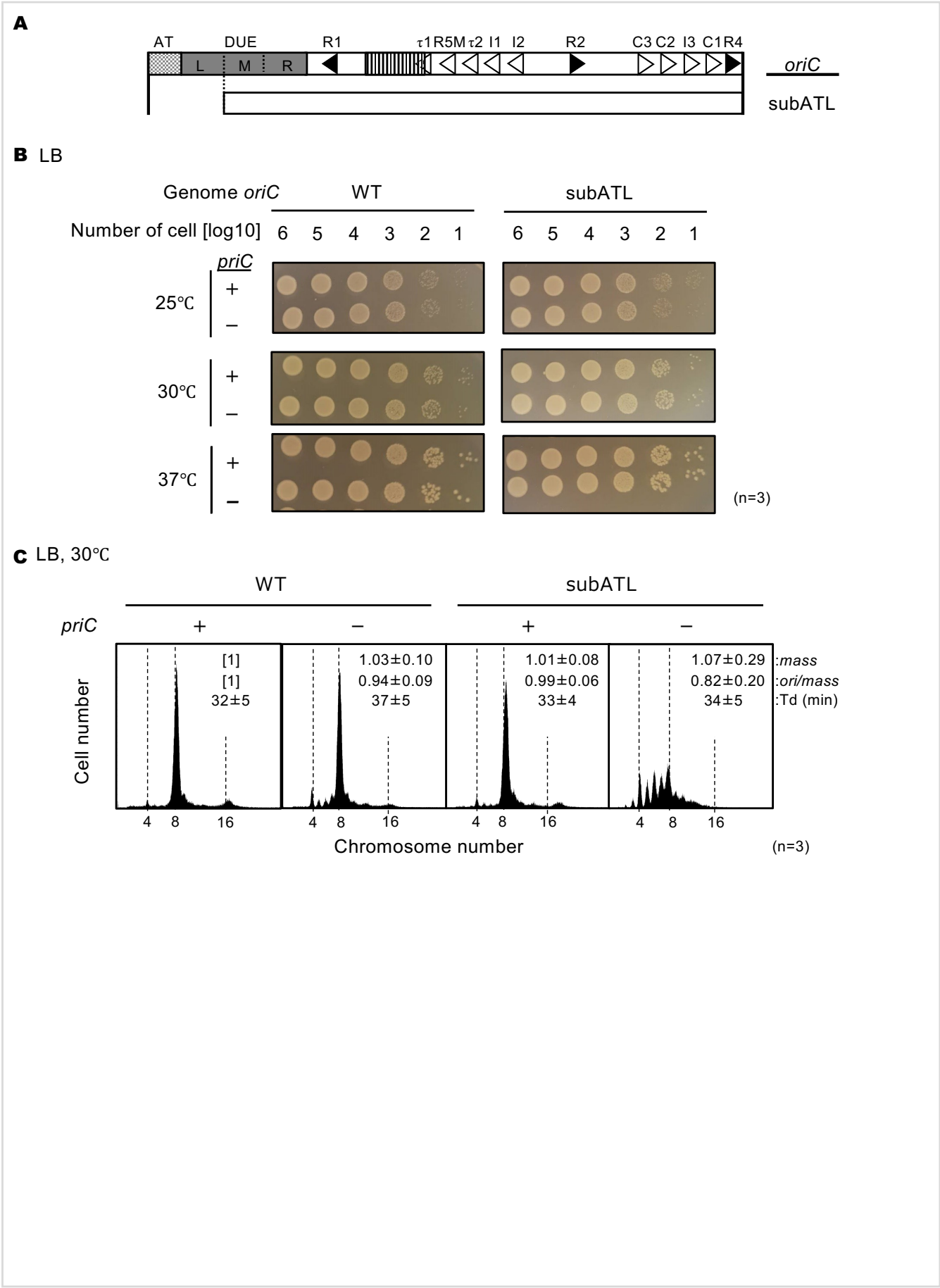
A
AT
DUE
R1
τ1 R5M τ2 I1 I2
R2
C3 C2 I3 C1 R4
L
M
R
oriC
subATL
B LB
Genome oriC
WT
subATL
Number of cell [log10]
6 5 4 3 2 1
6 5 4 3 2 1
priC
25℃
30℃
37℃
+
−
(n=3)
C LB, 30℃
WT
subATL
priC
+
−
+
−
[1]
[1]
32±5
1.03±0.10
0.94±0.09
37±5
1.01±0.08
0.99±0.06
33±4
1.07±0.29
0.82±0.20
34±5
:mass
:ori/mass
:Td (min)
Cell number
4 8 16
Chromosome number
(n=3)

Figure 7

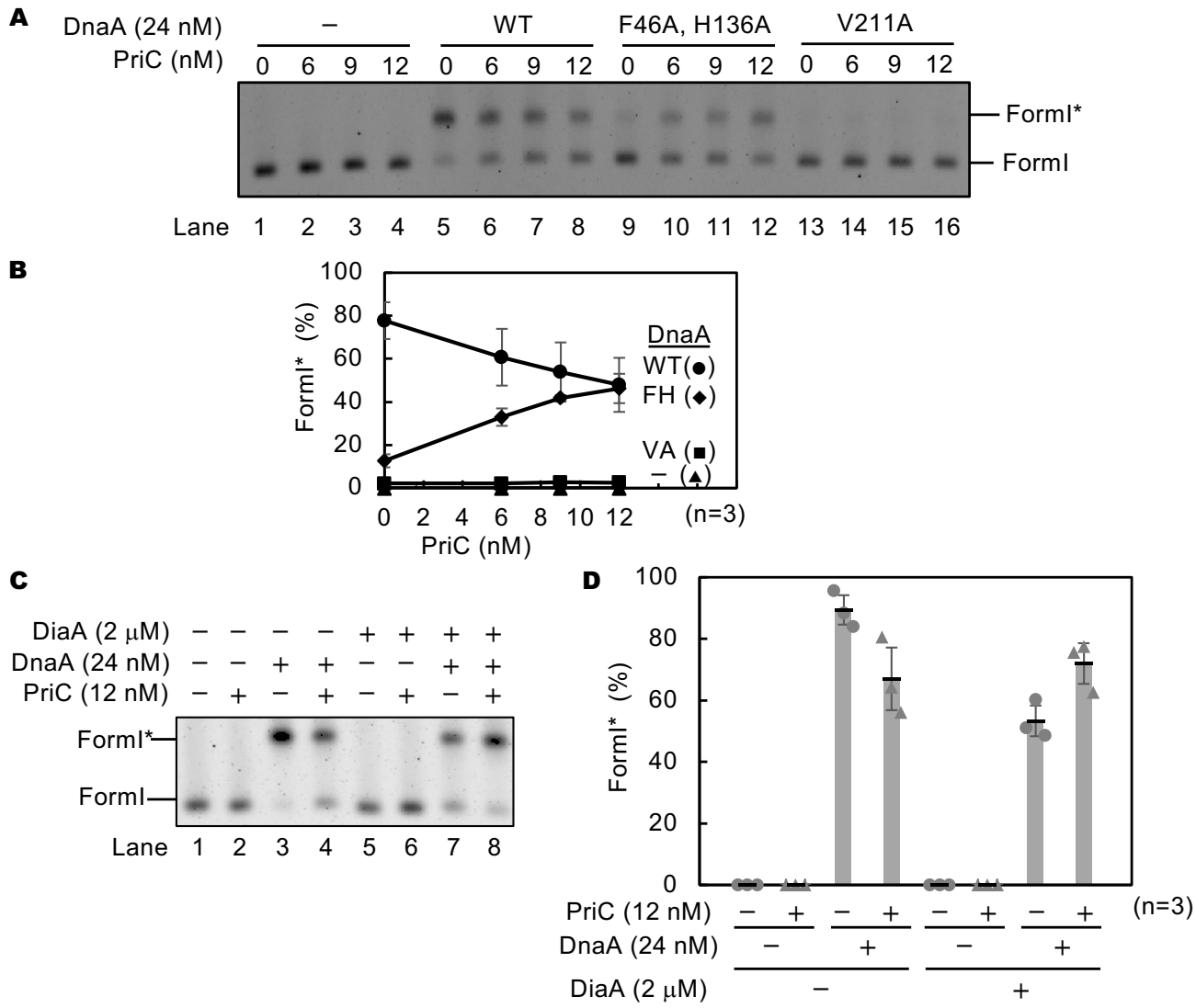
A
DnaA (24 nM)
PriC (nM)
–
WT
F46A, H136A
V211A
0 6 9 12 0 6 9 12 0 6 9 12 0 6 9 12
FormI*
FormI
Lane 1 2 3 4 5 6 7 8 9 10 11 12 13 14 15 16
B
FormI* (%)
100
80
60
40
20
0
DnaA
WT(●)
FH (◆)
VA (■)
– (▲)
0 2 4 6 8 10 12
PriC (nM)
(n=3)
C
DiaA (2 μM) – – – – + + + +
DnaA (24 nM) – – + + – – + +
PriC (12 nM) – + – + – + – +
FormI*
FormI
Lane 1 2 3 4 5 6 7 8
D
FormI* (%)
100
80
60
40
20
0
PriC (12 nM) – + – + – + – +
DnaA (24 nM) – + – +
DiaA (2 μM) – +
(n=3)

Figure 8

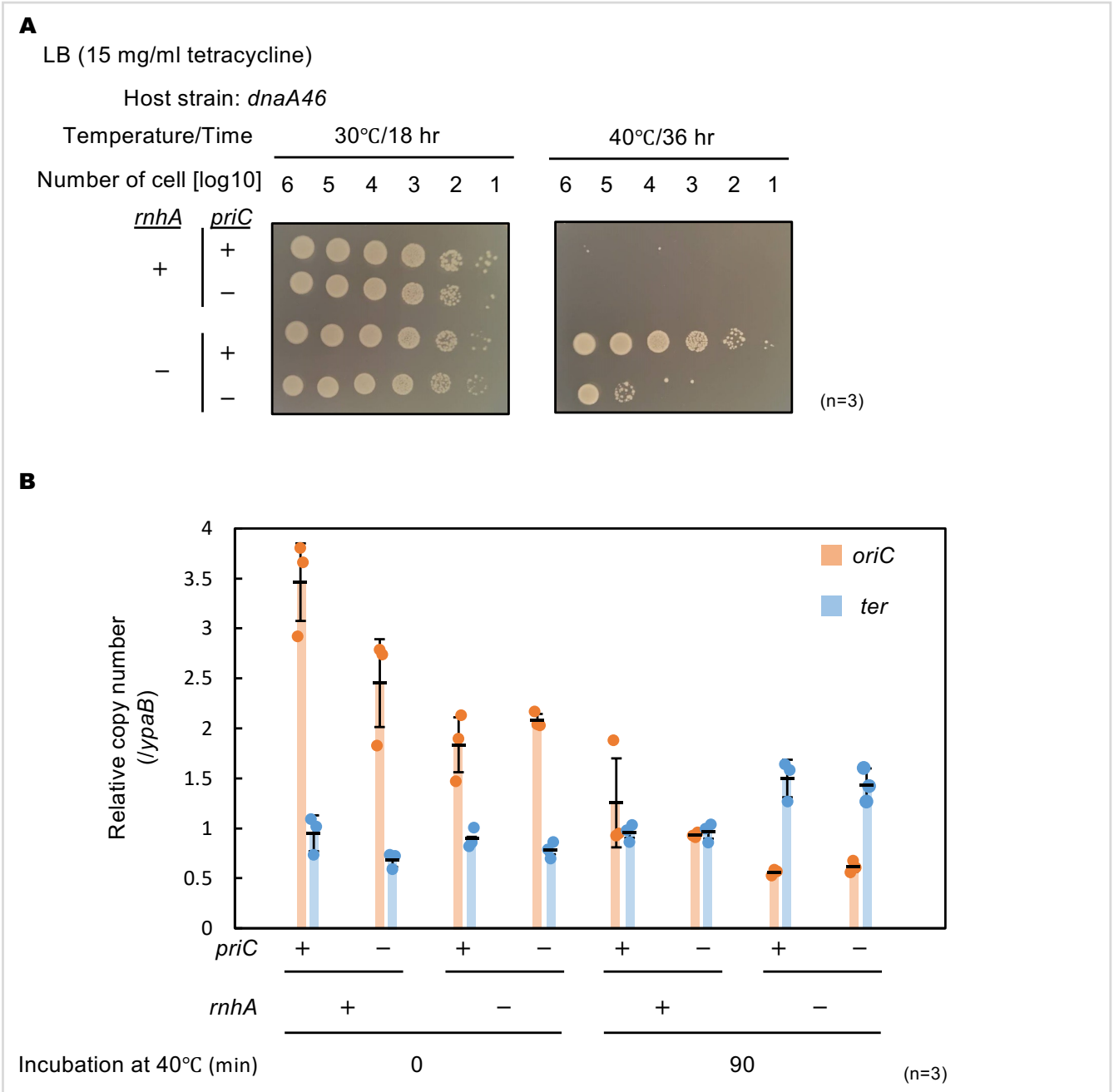
A
LB (15 mg/ml tetracycline)
Host strain: dnaA46
Temperature/Time
30℃/18 hr
40℃/36 hr
Number of cell [log10]
6 5 4 3 2 1
6 5 4 3 2 1
rnhA
priC
+
−
+
−
+
−
(n=3)
B
Relative copy number (/ypaB)
4
3.5
3
2.5
2
1.5
1
0.5
0
oriC
ter
priC
+ − + − + − + −
rnhA
+ − + −
Incubation at 40℃ (min)
0
90
(n=3)
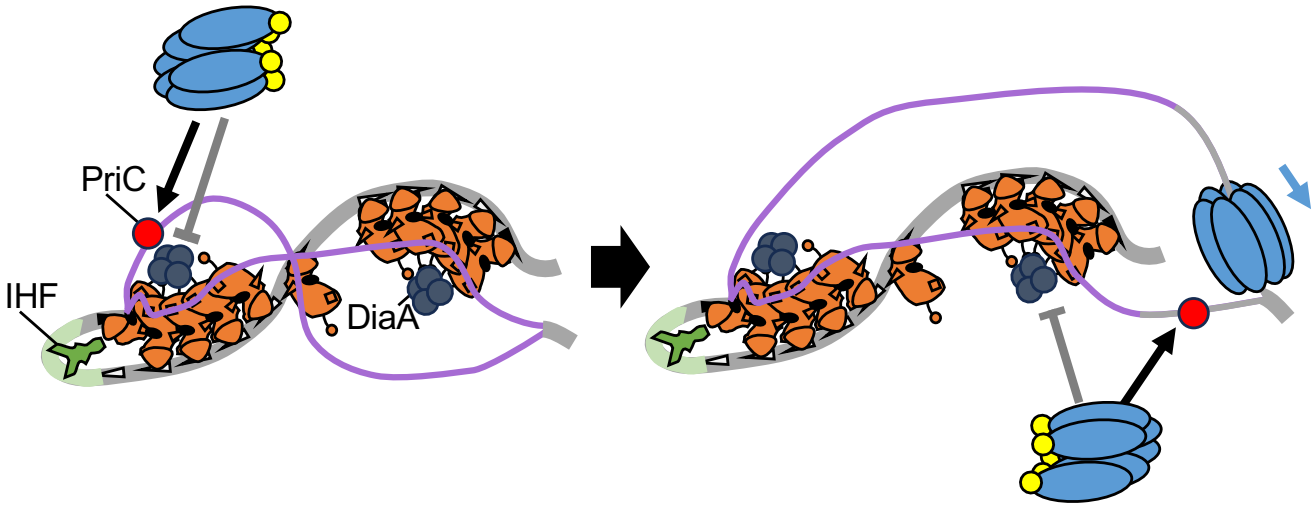
Figure 9